Characterization of Multi-Nuclear Manganese-Binding Bacterial Reaction Centers from *Rhodobacter sphaeroides*

by

Eduardo Espiritu

A Dissertation Presented in Partial Fulfillment
of the Requirements for the Degree
Doctor of Philosophy

Approved April 2019 by the
Graduate Supervisory Committee:

James P. Allen, Chair
Anne K. Jones
Kevin Redding

ARIZONA STATE UNIVERSITY

May 2019

ABSTRACT

In my thesis, I characterize multi-nuclear manganese cofactors in modified reaction centers from the bacterium *Rhodobacter sphaeroides*. I characterized interactions between a variety of secondary electron donors and modified reaction centers. In Chapter 1, I provide the research aims, background, and a summary of the chapters in my thesis. In Chapter 2 and Chapter 3, I present my work with artificial four-helix bundles as secondary electron donors to modified bacterial reaction centers. In Chapter 2, I characterize the binding and energetics of the P1 Mn-protein, as a secondary electron donor to modified reaction centers. In Chapter 3, I present the activity of a suite of four-helix bundles behaving as secondary electron donors to modified reaction centers. In Chapter 4, I characterize a suite of modified reaction centers designed to bind and oxidize manganese. I present work that characterizes bound manganese oxides as secondary electron donors to the oxidized bacteriochlorophyll dimer in modified reaction centers. In Chapter 5, I present my conclusions with a short description of future work in characterizing multiple electron transfers from a multi-nuclear manganese cofactor in modified reaction centers. To conclude, my thesis presents a characterization of a variety of secondary electron donors to modified reaction centers that establish the feasibility to characterize multiple turnovers from a multi-nuclear manganese cofactor.

DEDICATION

To Elena, Bonifacio, and Ivan Espiritu for their love and support.

ACKNOWLEDGMENTS

There are many people to be grateful for: my Mom, Dad, and younger Brother for always supporting me; Dr. James P. Allen and Dr. JoAnn C. Williams for their mentorship and their support of me as a graduate student; Dr. Anne K. Jones and Dr. Kevin Redding for being a part of my supervisory committee; Great friends of mine who are always around to help, such as, Dr. Chufeng Li, Yuhao Wang, Dr. Marco Flores, Dr. Tien L. Olson, Dr. Dong Wang, Dr. Andrew Serban, Dr. Christopher Gisriel, Zahra Bahrami Dizicheh, and Yifei Xu; Allen Lab members, such as, Kori Chamberlain, Dimah Abdullah, and Elizabeth Canarie; Thanks to Dr. Stewart Newfeld and the Initiative for Maximizing Student Development for funding parts of my thesis research; Many other people that I have met and am forgetting to list.

TABLE OF CONTENTS

Page

LIST OF TABLES

LIST OF FIGURES

LIST OF EQUATIONS

LIST OF ABBREVIATIONS

αMn_2O_3	Manganese oxide (III, III)
B	Bacteriochlorophyll *a*
H	Bacteriopheophytin *a*
$CaMn_2O_4$	Calcium-manganese oxide (III, III)
$P^+Q_A^-$	Charge-separated state
K_D	Dissociation constant
DF	*Due ferri*
P*	Excited state of the primary donor
Mn_4CaO_5	Manganese-calcium oxide cluster
$MnCl_2$	Manganese chloride
Mn_3O_4	Manganese oxide (II, III, III)
MnO_2	Manganese oxide (IV)
$Mn_3(PO_4)_2$	Manganese phosphate (II, II, II)
$E_m^{Mn(II)/Mn(III)}$	Mid-point potential of the Mn cofactor
O_2	Molecular oxygen
P^+	Oxidized bacteriochlorophyll dimer
$E_m^{P/P+}$	P/P^+ mid-point potential
PSII	Photosystem II

P	Primary donor
P680	Primary donor in photosystem II
Q_A	Primary quinone
Y_Z	Redox-active tyrosine
Q_A^-	Reduced primary quinone
Q_B	Terminal quinone
$Y_Z^\bullet$	Tyrosine radical

CHAPTER 1

INTRODUCTION

Research Aims

To meet the future global energy demand, developed and developing nations will require innovative technologies that produce energy that is renewable and carbon neutral.[1] Photo-electrochemical solar energy is identified as a potential source of renewable and carbon neutral energy.[2] The challenge in producing alternative energy is the need for technology that extracts electrons from sources that will feed into the production of a clean fuel, and water is identified as a source of electrons for fuel production.[3]

Biomolecules will serve as pivotal players in inspiring the next generation of catalysts for energy production.[4] There is a natural water oxidation catalyst in photosystem II (PSII). PSII is a membrane-bound protein-pigment complex that converts solar energy into chemical energy. PSII uses water as a substrate with an eventual release of molecular oxygen (O_2). PSII uses the manganese-calcium oxide cluster (Mn_4CaO_5) as the site of water oxidation and oxygen production. Many advances have been made to address the mechanisms of manganese oxidation in PSII, but not all catalytic steps are well understood, and it represents an open field of study.[5]

In my thesis, I address issues concerning manganese oxidation in PSII by characterizing manganese oxidation in modified bacterial reaction centers from *Rhodobacter sphaeroides*. The bacterial reaction center has been modified significantly to gain the functional capabilities of binding and oxidizing bound metal cofactors, a

feature that mimics PSII.[6] In this Chapter, I present a brief description of the following topics: photochemical reactions and protein structure of bacterial reaction centers, altered photochemical reactions in bacterial reaction centers, manganese chemistry, metal-binding bacterial reaction centers, and absorption spectra of bacterial reaction centers.

Photochemical reactions and protein structure of bacterial reaction centers

The reaction center is the core component in photosynthesis, and the reaction center is responsible for the primary conversion of solar energy to chemical energy. The photosynthetic reaction centers have two different classifications: the iron-sulfur reaction center and the pheophytin-quinone reaction center.[7] The reaction centers from *Rhodobacter sphaeroides* and PSII are both pheophytin-quinone type reaction centers with different sets of pigments.

The photochemical reaction starts with an absorption of a photon by the primary donor (P) forming an excited state of the primary donor (P*). P in bacterial reaction centers is a dimer of bacteriochlorophyll *a* (B) molecules with edge-to-edge contact making the electrons delocalized between the two molecules.[7] The forward electron transfer in bacterial reaction centers proceeds from P* to a bacteriopheophytin *a* molecule (H) on the active electron transfer branch (H_A), leading to the charge-separated state $P^+H_A^-$. The electron on H_A^- is then transferred to the primary quinone (Q_A) yielding the charge-separated state $P^+Q_A^-$, and finally, the electron on Q_A^- proceeds to the terminal quinone (Q_B) yielding the charge-separated state $P^+Q_B^-$ (Figure 1.1).[8] In *Rhodobacter sphaeroides*, cytochrome c_2 is a secondary electron donor to P^+ making it possible for absorption of a second photon and subsequent transfer of a second electron to Q_B^-.

Coupling with proton uptake yields Q_BH_2, which is released from bacterial reaction centers into a quinone/quinol pool.[9]

The pigments in PSII are chlorophyll *a* and pheophytin *a* molecules, which are different from B and H in bacterial reaction centers. The primary donor in PSII has an absorption maximum at 680 nm (P680), making use of higher energy photons relative to the absorption maximum of 865 nm for P from bacterial reaction centers.[6] After absorption of a photon and formation of the charge-separated state $P680^+Q_B^-$, a redox-active tyrosine (Y_Z) reduces the $P680^+$ leaving a tyrosine radical ($Y_Z^\bullet$), which in turn is reduced by the Mn_4CaO_5 cluster.[5] The S cycles detail the known oxidation states of the Mn_4CaO_5, which ultimately uses water as substrate and leads to an eventual release of O_2.[10]

The reaction center from *R. sphaeroides* falls under the classification of an asymmetric reaction center because of the hetero dimer protein structure.[6] The L and M subunits are the core of the bacterial reaction center, and each subunit has five trans-membrane helices; the H subunit is anchored to the membrane by a single membrane-bound helix, and the H subunit is exposed to the cell cytoplasm (Figure 1.2).[11] The electron transport chain comprised of the A-branch and B-branch has the following pigments: B_A, H_A, Q_A, B_B, H_B and Q_B.[12] P is positioned near the periplasmic surface of the membrane, and the quinone molecules are positioned near the cytoplasmic surface of the membrane.[13] In comparison, PSII has a larger number of subunits, and the PSII reaction center is asymmetric with the D1 and D2 subunits at the core binding the electron transport chain.[6]

Altered photochemical reactions in bacterial reaction centers

A functional difference between bacterial reaction centers and PSII is the mid-point potential of the primary donor, as P680 in PSII has a mid-point potential of approximately 1.0 V and P in the reaction centers from *R. sphaeroides* has a mid-point potential of 0.5 V.[6,10] To increase the P/P^+ mid-point potential in the reaction centers, histidine residues are incorporated to the reaction center protein structure, forming hydrogen bonds that stabilize P.[14] The residues Leu L131, Leu M160 and Phe M197 are changed to histidine, and the addition of a single histidine at positions L131, M160 and M197 yielding increases of 80, 60 and 125 mV, respectively, in the P/P^+ mid-point potential relative to the wild-type reaction center.[14] Furthermore, a set of double mutants and a triple mutant reaction center with histidine modifications make up the following possible combinations: LH L131 and LH M160, LH L131 and FH M197, LH M160 and FH M197, and LH L131, LH M160, and FH M197 (also called HHHH or T1), and the increases in P/P^+ mid-point potentials relative to the wild-type reaction center are as follows: 130, 210, 200 and 260 mV, respectively (Figure 1.3).[14-16] The mutant bacterial reaction centers exhibit altered reaction rates in comparison to the wild-type reaction center. For example, the $P^+Q_A^-$ charge-recombination time in the LH L131, LH M160, and FH M197 reaction center is 40 ms in comparison to 100 ms in the wild-type, because the free energy difference between the $P^+Q_A^-$ state and the ground state is increased in the mutant (Figure 1.4).[14] All the while, the mutant reaction centers have gained the functional capability of extracting electrons from secondary donors other than

cytochrome c_2, the natural secondary donor, due to the larger P/P^+ mid-point potentials.[15, 16]

Manganese chemistry

Manganese is a suitable metal for water oxidation because the oxidation states of Mn(III) and Mn(IV) have large mid-point potentials in Mn-compounds with μ-oxo-bridges stabilizing Mn(III) and Mn(IV).[17] In solution, Mn(II) is stable, and Mn(II) hexa-hydrate is difficult to oxidize because the $3d^5$ electronic configuration does not favor a transition to the $3d^4$ electronic configuration.[18] In solution, Mn(III) is unstable, so it undergoes disproportionation to Mn(II) and Mn(IV). MnO_2, with the oxidation state of Mn(IV), is a compound that is thermodynamically stable, and it is insoluble in aqueous solutions.[19] Mn compounds with mixed oxidation states of Mn(III) and Mn(IV) are stabilized by organic ligands, and chemical characterization of the compounds in the presence of a strong oxidant exhibit capabilities of water oxidation.[20,21] Mn containing enzymes, such as Mn-superoxide dismutase and Mn-catalase are demonstrations of Mn involvement in a broad scope of catalytic functions.[10] The Mn cluster in PSII effectively facilitates the four proton-coupled electron transfer events to oxidize water due to the suitable range of oxidation states of the cluster.[22]

Metal-binding bacterial reaction centers

PSII has the Mn_4CaO_5 complex that enables water oxidation, but the wild-type bacterial reaction centers are not capable of binding or oxidizing the transition metal manganese.[16] I described the structural modifications in bacterial reaction centers that enable manganese oxidation in a previous section. In this section, I describe the

modifications that enable manganese binding. In the photo-activation process of PSII, the first step is the binding of a Mn(II) ion in a high-affinity binding site with Asp 170 of the D1 subunit being involved.[5] In wild-type bacterial reaction centers, Glu M173 is the amino acid at the homologous position.[23] Three amino acids were identified near Glu M173 to substitute with carboxylate amino acids for binding metals: Met M168, Val M192 and Gly M288. A mutant capable of manganese binding and oxidation was the M2 reaction center, also termed the Mn12 reaction center, based on the criterion of a high affinity for Mn(II).[24] The M2 mutant has the modifications for a high P/P^+ mid-point potential, a modification from Arg M164 to Tyr, and modifications of Met M168 to Glu and Gly M288 to Asp for binding metals.[24,25] The binding site is strategically positioned 10 Å from P for efficient incorporation of exogenous Mn(II) and efficient electron transfer from a bound Mn(II) cofactor (Figure 1.5). The energetics of the Mn(II) electron transfer to P^+ in reaction centers is characterized with variants of the M2 mutants with a range of P/P^+ mid-point potentials.[25] The versatility of the binding site allowed for addition of Fe(II) as a bound cofactor.[26]

Absorption spectra of bacterial reaction centers

Absorption spectroscopy is a useful technique that allows correlation of the optical changes in bacterial reaction centers to specific states of electron transfer. Absorption by a sample is dependent on the path length, the concentration of the chemical species, and the molar absorptivity of the chemical species.

In the near-infrared regions, wild-type bacterial reaction centers have three distinct absorption peaks at 760 nm, 800 nm and 865 nm, that are attributed to the H, B and P

pigments, respectively (Figure 1.6). Also shown in Figure 1.6 is a light-minus-dark optical spectrum of wild-type reaction centers with terbutryne, an inhibitor of electron transfer to Q_B. This experiment is a steady-state measurement of reaction centers under continuous illumination with sub-saturating light that bleaches 20 % of P in the wild-type reaction center. A decrease in absorption at 865 nm is due to a loss in absorption of P consistent with formation of P^+. The increase in absorption at 770 nm is consistent with electrochromic shifts in the H and B bands as a result of the formation of Q_A^-. The light-minus-dark experiment is useful for characterization of electron transfer from secondary electron donors to P^+ with steady-state conditions.

Thesis projects

To build on the modifications of the bacterial reaction centers for binding and oxidizing a Mn(II) ion, my thesis explores the binding and oxidation of multi-nuclear Mn cofactors in modified bacterial reaction centers. Initially, I set out to establish exogenous artificial Mn-proteins as suitable secondary electron donors to P^+ in reaction centers. The artificial Mn-proteins are inspired by the *due ferri* (DF) proteins designed by DeGrado and coworkers.[27] In Chapter 2, I present a detailed characterization of Mn-protein binding to the reaction center and the energetics of electron transfer. In Chapter 3, I present a survey of electron transfer from several Mn-proteins to reaction centers. A second project I worked on is characterization of electron transfer from bound Mn in structurally modified reaction centers. The identification of the ligands binding the Mn_4CaO_5 cluster as revealed in the PSII structure helped to inspire the modifications made in bacterial reaction centers.[22] In Chapter 4, I show the incorporation of Mn oxides in metal-binding

bacterial reaction centers. The complete scope of my thesis is to show the incorporation and oxidation of multi-nuclear manganese cofactors in modified bacterial reaction centers. I also contributed to projects that studied energy transfer in reaction centers, which is not included in the thesis.[28]

Figures

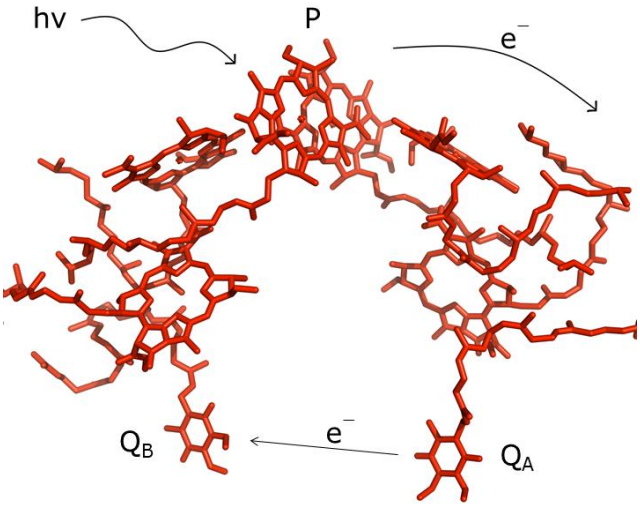

Figure 1.1. Electron transfer scheme in the bacterial reaction center from *R. sphaeroides*. The bacteriochlorophyll *a* dimer (P) absorbs a photon and following excitation to P*, electron transfer follows through the A-branch, as shown by the arrow on the top right corner of the figure. Initially, the electron is transferred from P to the primary quinone (Q_A) yielding a charge-separated state $P^+Q_A^-$. Finally, the electron is transferred to the terminal quinone (Q_B) yielding a charge-separated state $P^+Q_B^-$. The cofactors are shown in red and the arrow shows the direction of electron transfer. The structure is from the variant M2 reaction center from *R. sphaeroides* with a PDB ID of 1Z9J.

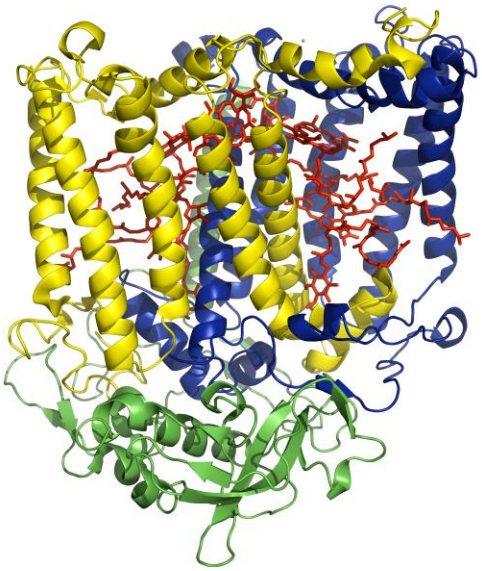

Figure 1.2. Schematic structure of the M2 reaction center from *R. sphaeroides*. The reaction center is a membrane-bound protein with the L subunit (yellow) and the M subunit (blue) being trans-membrane subunits. The cofactors (red) are bound to the L and M subunits with the bacteriochlorophyll *a* dimer positioned near the periplasmic surface. The H subunit (green) is anchored to the membrane by a membrane-bound helix. The H subunit is positioned in the cell cytoplasm. The structure is of the variant M2 reaction center from *R. sphaeroides* with a PDB ID of 1Z9J.

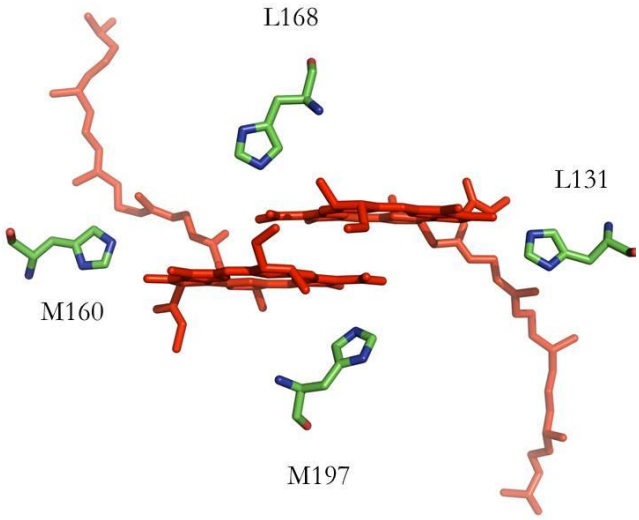

Figure 1.3. The structure of the bacteriochlorophyll *a* dimer with the modifications of histidines at positions M160, L131, and M197. The histidine amino acids are shown based on the color of the different atoms with carbon in green, oxygen in red, and nitrogen in blue. The bacteriochlorophyll *a* dimer is shown in red. The structure is from the variant M2 reaction center from *Rhodobacter sphaeroides* with a PDB ID of 1Z9J.

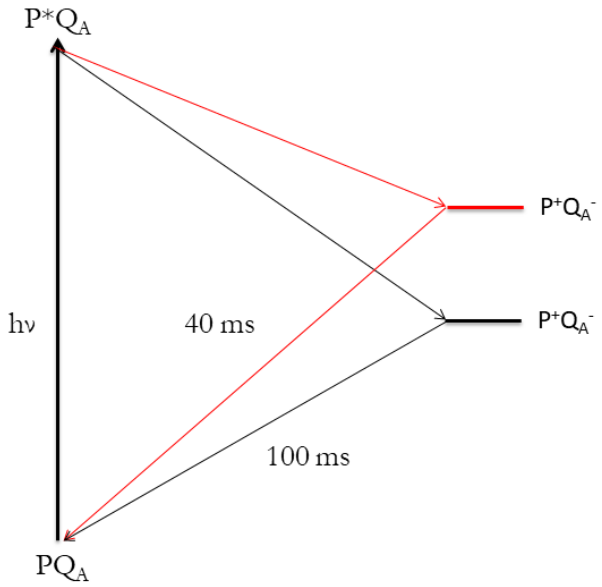

Figure 1.4. Energy-level diagrams of $P^+Q_A^-$ and charge recombination rates. Absorption of a photon by reaction centers (PQ_A) yields the excited state P^*Q_A, and subsequent formation of the charge-separated state, $P^+Q_A^-$. The recombination time of 100 ms in the wild-type reaction center (black) is slower than the 40 ms recombination time in the LH L131, LH M160, and FH M197 reaction center (red).

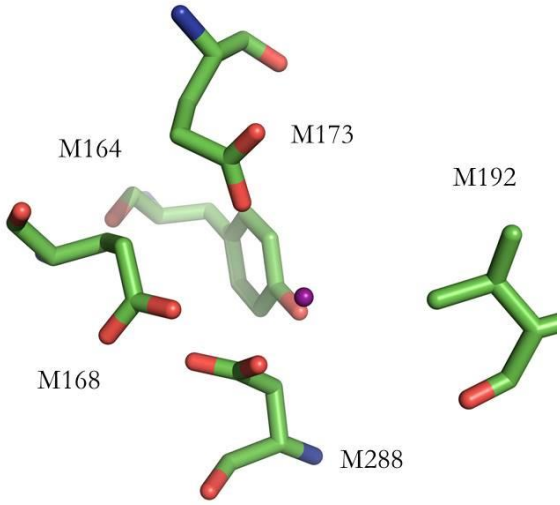

Figure 1.5. The structure of the manganese-binding site in M2 reaction centers. The manganese-binding site includes the following modifications: Arg to Tyr M164, Met to Glu M168, and Gly to Asp M288. Glu M173 and Val M192 are amino acids that are in the native reaction centers. The carbon atoms are shown in green, nitrogen is in blue, oxygen is in red, and manganese is in purple. The structure is from the variant M2 reaction center from *Rhodobacter sphaeroides* with a PDB ID of 1Z9J.

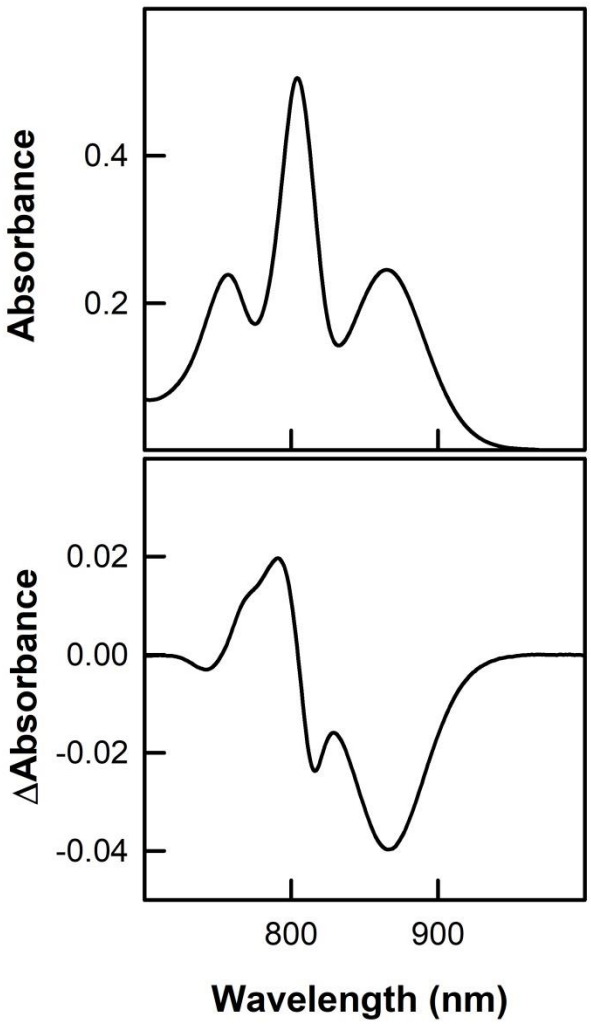

Figure 1.6. The near-infrared absorption spectrum of the wild-type bacterial reaction center (top panel) and the light-minus-dark difference absorption spectrum of the wild-type reaction center with terbutryne (bottom panel). The wild-type reaction center absorption spectrum has three distinct peaks centered at 760 nm, 800 nm, and 865 nm that are representative of H, B, and P, respectively. The light-minus-dark spectrum of wild-type reaction centers with the inhibitor terbutryne shows a decrease in absorption at 865 nm. The decrease in absorption at 865 nm is correlated to a loss of P and is consistent with formation of P^+. The increase in absorption at 770 nm is correlated with electrochromic shifts in the H and B bands and is consistent with formation of Q_A^-. Conditions: 1.5 μM wild-type reaction centers in 15 mM N-cyclohexyl-2-aminoethanesulfonic acid pH 9.4, 0.025 % Triton X-100 and 100 μM terbutryne.

CHAPTER 2

BINDING AND ENERGENTICS OF ELECTRON TRANSFER BETWEEN AN ARTIFICIAL FOUR-HELIX MN-PROTEIN AND REACTION CENTERS FROM RHODOBACTER SPHAEROIDES

The work I completed for the publication was characterization of the binding and energetics from the electron transfer from the Artificial Mn-protein to the modified reaction centers. I used light-minus-dark optical spectroscopy to characterize the electron transfer reactions. The data I collected was analyzed by me. Additionally, I made the data figures for the paper. I wrote parts of the introduction, materials and methods, and results.

Abstract

The ability of an artificial four-helix bundle Mn-protein, P1, to bind and transfer an electron to photosynthetic reaction centers from the purple bacterium *Rhodobacter sphaeroides* was characterized using optical spectroscopy. Upon illumination of reaction centers, an electron is transferred from P, the bacteriochlorophyll dimer, to Q_A, the primary electron acceptor. The P1 Mn-protein can bind to the reaction center and reduce the oxidized bacteriochlorophyll dimer, P^+, with a dissociation constant of 1.2 μM at pH 9.4, comparable to the binding constant of *c*-type cytochromes. Amino acid substitutions of surface residues on the Mn-protein resulted in increases in the dissociation constant to 8.3 μM. The extent of P^+ reduction by the P1 Mn-protein was dependent on the P/P^+ midpoint potential and the pH. Analysis of the free energy difference yielded a midpoint potential of approximately 635 mV at pH 9.4 for the Mn cofactor of the P1 Mn-protein, a value similar to those found for other Mn-cofactors in proteins. The linear dependence of –56 mV/pH is consistent with one proton being released upon Mn oxidation, allowing the complex to maintain overall charge neutrality. These outcomes demonstrate the feasibility of designing four-helix bundles and other artificial metalloproteins to bind and transfer electrons to bacterial reaction centers and establish the usefulness of this system as a platform for designing sites to bind novel metal cofactors capable of performing complex oxidation/reduction reactions.

Introduction

Mn-based oxidation/reduction reactions play significant roles in biology, with multinuclear Mn- clusters being capable of achieving multiple oxidation states that are

coupled with a range of electron and proton transfer processes.[18] For example, Mn-enzymes facilitate oxygen-atom transfer processes as performed by Mn-superoxide dismutase, Mn-catalase, and photosystem II.[29] To understand the mechanism of these reactions, biomimetic compounds can be manipulated with different ligands, and artificial protein complexes can be designed with metal centers capable of electron transfer.[30–36] Advancements in the field of protein design using a minimal protein scaffold has led to functional artificial proteins that facilitate an array of enzymatic reactions depending on the protein sequence.[27,32,37,38] To investigate light-triggered electron transfer steps involving Mn-cofactors, we are combining artificial four-helix bundles containing dinuclear Mn-centers with bacterial reaction centers. In this paper we address in a quantitative way the characteristics of this system, in particular the binding and energetics of electron transfer from Mn-centers of four-helix bundles to reaction centers.

The reaction center from *Rhodobacter sphaeroides* is a membrane-bound pigment-protein complex responsible for converting light energy into chemical energy.[39] In these bacteria, electron transfer is coupled to proton transport across the cell membrane in a cycle involving the reaction center, cytochrome bc_1 complex and cytochrome c_2. In the reaction center, the absorption of light by a bacteriochlorophyll dimer, P, initiates electron transfer through intermediate electron acceptors to the primary quinone, Q_A (Figure 2.1). The reduced primary quinone, Q_A^-, then transfers the electron to the secondary quinone, Q_B. The natural secondary electron donor to P^+ is a water-soluble cytochrome c_2, which transiently binds to the periplasmic surface of the reaction center.[40,41] After reduction of P^+, a second photon absorption and electron transfer can

take place, with the doubly-reduced Q_B being protonated and exchanged with the quinone pool in the membrane. The cytochrome bc_1 complex acts as an oxidoreductase, removing the protons and electrons from the quinol, releasing the protons to the other side of the membrane, and reducing cytochrome c_2.[42] In other photosynthetic organisms, the electron transfer process is linear, with a terminal electron donor and acceptor, most notably in oxygenic photosynthesis, where the terminal electron donor water is oxidized by photosystem II, which is evolutionarily related to the reaction center in *R. sphaeroides*.

The capability for oxidation reactions by the reaction center is established by the P/P^+ midpoint potential, $E_m^{P/P+}$, which is approximately 500 mV in wild-type reaction centers.[14] For example, in photosystem II the primary electron donor, P680, has a midpoint potential that is over 500 mV higher than that of the primary electron donor P in the bacterial reaction center, enabling the oxidation of water through the Mn_4CaO_5 cluster. In reaction centers, the value of $E_m^{P/P+}$ is sensitive to interactions with residues from the L and M transmembrane subunits, which constitute the core of the reaction center protein, and both electrostatic interactions with ionizable residues and hydrogen bonds from amino acid residues to the conjugated macrocyle have been shown to influence $E_m^{P/P+}$.[43] Alterations of several hundred mV can be obtained by combinations of mutations at four positions, L131, L168, M160 and M197, where His, Glu and Asp can form hydrogen bonds with P (Figure 2.2).[14,44] In wild-type reaction centers, after binding of cytochrome c_2, P^+ is efficiently reduced by an electron-transfer reaction with a free energy difference of –160 meV, corresponding to the difference between $E_m^{P/P+}$ and the midpoint potentials of the heme group of the cytochrome c_2.[45] Wild-type reaction centers

are unable to oxidize Mn, but for reaction centers with higher values of $E_m^{P/P+}$, the oxidation of additional secondary donors such as Mn becomes possible (Figure 2.3).[24]

The highly-oxidizing reaction centers are capable of electron transfer from Mn-cofactors that are either bound at an introduced site on the M subunit or contained in exogenous artificial Mn-proteins.[24,46,47] Members of the DF (*due ferri*) protein family of artificial proteins form four-helix bundles with a central dinuclear metal cluster capable of binding Fe and Mn, as well as other metals.[27,32,37,38] Our four-helix bundle Mn-protein designated P1 is based on the DF protein family, with significant modifications to include two additional dinuclear metal-binding sites.[46–48] The P1 Mn-protein is modeled as binding to the reaction center and undergoing electron transfer reactions similar to those involving cytochrome c_2 (Figure 2.1). This interaction, the formation of the Mn-protein-reaction center complex and the energetics of electron transfer from Mn(II) to P^+ after illumination of the complex:

$$\mathrm{P1Mn(II)} + \mathrm{PQ_A} \overset{K_D}{\Leftrightarrow} \mathrm{P1Mn(II):PQ_A} \overset{h\nu}{\rightarrow} \mathrm{P1Mn(II):P^+Q_A^-} \overset{\Delta G^\circ}{\Leftrightarrow} \mathrm{P1Mn(III):PQ_A^-} \qquad (2.1)$$

The strength of the binding of the Mn-protein to the reaction center is described by the dissociation constant, K_D. The reduction of P^+ is driven by the free energy difference, $\Delta G°$, which is related to the difference between $E_m^{P/P+}$ and the midpoint potential of the Mn cofactor, $E_m^{Mn(II)/Mn(III)}$. To simplify the reactions in this case, electron transfer to the secondary quinone is blocked by the addition of terbutryne.

In this report, we characterize the properties of the transfer of an electron from the P1 Mn-protein to the reaction center. The energetics of the transfer were investigated by measuring the extent of the electron transfer to reaction centers modified to have different

values of $E_m^{P/P+}$, ranging from 468 to 748 mV at pH 9.4.[14,49] We measured the binding and yield of electron transfer for different combinations of Mn-proteins with altered surface residues and reaction centers with substitutions near P, as well as the pH dependence of K_D and $E_m^{Mn(II)/Mn(III)}$. The characteristics of the binding of the Mn-proteins to the reaction centers and the energetics of electron transfer are compared to the native secondary donor, cytochrome c_2, and natural Mn-proteins.

Materials and Methods

Preparation of reaction centers. The reaction centers from wild type and mutants with altered hydrogen bonds to P have been described.[14,44] The wild-type reaction centers have four amino acid residues, Leu L131, His L168, Leu M160, and Phe M197 (forming the tetrad LHLF), in positions for forming hydrogen bonds to the conjugated system of P (Figure 2.2). These residues were altered to Asp, Glu, or His, and the nomenclature for the strains in this paper identifies the residues at these four positions. For example, reaction centers with the changes Leu L131 to His and Leu M160 to His are designated HHHF, and those with the changes Leu L131 to His, Leu M160 to His, and Phe M197 to His are named HHHH.

Reaction centers were prepared as previously described[24] and stored at –80°C in 15 mM Tris(hydroxymethyl)aminomethane-hydrochloride (Tris-HCl) (pH 8.0) and 0.05 % Triton X-100. To equilibrate the reaction centers at the appropriate pH, the reaction center stock in 15 mM Tris-HCl (pH 8.0) and 0.05 % Triton X-100 was diluted 50-fold into 15 mM buffer (Tris-HCl for pH 8.4 to 8.6 or N-cyclohexyl-2-aminoethanesulfonic acid (CHES) for pH 8.8 to 9.6) and 0.025 % Triton X-100. The reaction centers were then

concentrated using Amicon 30000 molecular weight cutoff (MWCO) centrifugal filters with a CL2 centrifuge at 3600 rpm (ThermoFisher Scientific).

Preparation of P1, P1-1, and P1-2 Mn-proteins. The construction of the P1 protein has been reported previously.[46–48] The genes encoding the P1-1 and P1-2 proteins were derived from the gene for the P1 protein by oligonucleotide-directed mutagenesis. The P1-1 protein contains the changes Glu 20 (GAA) to Lys (AAA) and Glu 23 (GAA) to Lys (AAG). The P1-2 protein contains the changes Asp 2 (GAC) to Arg (CGT) and Asn 27 (AAC) to Lys (AAA). The artificial proteins are expressed in *Escherichia coli* and contain a six-His tag for purification by immobilized metal affinity chromatography. A TEV protease recognition site is incorporated for removal of the six-His tag after the affinity column purification.

For purification, frozen cell pellets were suspended in 20 mM sodium phosphate (pH 7.4), 20 mM imidazole, and 500 mM NaCl. The cells were lysed with a French pressure cell, and the lysate was immediately centrifuged for 60 min at 4°C at 24500 x *g* in a Sorvall RC6 Plus centrifuge with a SA-600 rotor (ThermoFisher Scientific). The supernatant containing the soluble artificial protein was incubated with Ni Sepharose 6 Fast Flow slurry (GE Healthcare) for 120 min at 4°C and then loaded into a 2-cm diameter glass column. After being washed with 20 mM sodium phosphate (pH 7.4), 30 mM imidazole and 500 mM NaCl, the protein was eluted with 20 mM sodium phosphate (pH 7.4), 300 mM imidazole, and 500 mM NaCl. To cleave the six-His tag from the protein, TEV protease, 20 µg for every 100 µg of artificial protein, and *β*-mercaptoethanol, at a final concentration of 14 mM, were added to the sample, with the

protein amount calculated using an extinction coefficient at 280 nm for the full-length expressed protein monomer of 10.0 $mM^{-1}cm^{-1}$. After the sample was incubated at 4°C overnight, the imidazole concentration was decreased via dialysis against 20 mM sodium phosphate and 300 mM NaCl, using 1000 Da MWCO dialysis tubing. After dialysis, the sample was incubated with Ni Sepharose for 90 min, followed by the addition of imidazole to a final concentration of 20 mM. After being mixed for 30 min, the sample was loaded onto a glass column to remove the amino-terminal portion of the protein containing the six-His tag, which bound to the Ni-NTA resin, as the artificial protein did not bind and was collected in the flow-through. The solution with the artificial protein was analyzed by sodium dodecyl sulfate-polyacrylamide gel electrophoresis to determine if the cleavage and separation were complete. The sample was dialyzed against ultra-pure water using 1000 Da MWCO tubing and then stored at –80°C. An extinction coefficient at 280 nm of 4.2 $mM^{-1}cm^{-1}$ was used to determine the concentration of the artificial protein dimer.

To bind Mn, the protein at a concentration of 15 μM was mixed with 135 μM $MnCl_2$ in 5 mL of water for 10 min at 4°C. The sample was concentrated 8-fold by centrifugation in a CL2 centrifuge at 3600 rpm and 4°C using Amicon 3000 MWCO centrifugal filters. The sample was then diluted to the original volume, and $MnCl_2$ was added to a final concentration of 135 μM to the diluted artificial protein. After being mixed for 10 min at 4°C and concentrated 8-fold again, the sample was diluted 5-fold and incubated overnight. Following the overnight incubation, the Mn-protein was

concentrated to 350-600 μM for use in titrations with reaction centers. Electron paramagnetic resonance spectroscopy has been used to verify the binding of the Mn.[46,47]

Determination of optical changes. Light-induced spectral changes of the reaction center were measured using Varian Cary 5 and Varian Cary 6000i ultraviolet-visible-near spectrometers (Agilent Technologies). For the light-minus-dark spectra, the reaction centers were illuminated using sub-saturating light from a 1000-W tungsten bulb with an 860 nm interference filter as described previously.[24] The kinetic measurements were performed using saturating 1 ns pulses at 532 nm from a Surelite SLI-10 Nd:YAG laser (Continuum).

Determination of dissociation constants. Titrations of the Mn-proteins to the reaction centers were used to determine the dissociation constant for binding as described previously.[25] The starting reaction center concentration was 1.5 μM in 15 mM buffer (Tris-HCl for pH 8.4 to 8.6, or CHES for pH 8.8 to 9.6), 0.03 % Triton X-100 and 100 μM terbutryne in a starting volume of 750 μL. The Mn-protein was added stepwise at final concentrations ranging from 0.175 to 17.5 μM. At each concentration of the Mn-protein, a light-minus-dark spectrum was measured from 700 to 1000 nm, with the spectrum in the dark prior to illumination as the baseline. The sample was illuminated for duration of the scan. Immediately after the illuminated scan, a prompt-minus-dark spectrum was taken of the sample in the dark. After 5 min, a recovery spectrum of the sample was recorded. For data analysis the prompt-minus-dark spectrum was subtracted from the light-minus-dark spectrum to remove any contribution from long-lived charge-

separated states that the reaction center sample might incur after prolonged illumination. At least three titrations were performed for each condition.

For second-order electron transfer, the dissociation constant, K_D is determined by the concentration of the unbound donor and acceptor. If the free and bound concentrations are experimentally observable, the value of K_D can then be determined from these concentrations, as, for example has been done for binding of cytochrome c_2 to the reaction center using the relative amplitudes of kinetic signals associated with the absorption spectra of these two proteins.[50,51] The measurements presented in this work do not distinguish the free and bound concentrations of Mn, requiring the K_D for binding of Mn-protein to the reaction center be determined using a relationship involving the total Mn concentration. In this case, K_D is a measure of the amount of the P1Mn(II):PQ_A complex compared to the amount of P1Mn(II) and PQ_A separately in solution (Equation 2.1). The optical assay measures the formation of the complex indirectly through the amount of reaction centers in the $P^+Q_A^-$ state. For this analysis, the extent of bleaching of P in the reaction center in the presence of Mn-protein was monitored at 865 nm, ΔA^{M}_{865nm}. To quantify the relative P^+ fraction, the extent of bleaching at each Mn-protein concentration was initially normalized to the absorption change at the lowest Mn-protein concentration, 0.175 μM:

$$\text{relative } P^+\text{fraction} = \frac{\Delta A^{M}_{865nm}}{\Delta A^{0.175}_{865nm}} \quad (2.2)$$

The relative P^+ fraction over the course of the titration can be described in terms of the total concentration of the Mn-protein, $[Mn]_t$ and K_D by adapting a relationship previously described (Supplemental Information):

$$\text{relative } P^{+}\text{fraction} = A\left(\frac{([RC]_t-[Mn]_t-K_D)\pm\sqrt{([Mn]_t-[RC]_t+K_D)^2+4[RC]_tK_D}}{2\,[RC]_t}\right)+B \quad (2.3)$$

where $[RC]_t$ is the total concentration of the reaction center and *A* and *B* describe the limiting values for the relative P^+ fraction that is reduced by the Mn-protein and that remains oxidized at high concentrations of the Mn-protein, respectively.[24,52] The sum of *A* and *B* was constrained to be 1 and was used for renormalization of the relative P^+ fraction. The reaction center concentration for the titrations was set at 1.5 μM.

Determination of the Mn(II)/Mn(III) midpoint potential. The $E_m^{Mn(II)/Mn(III)}$ was determined as previously described on the basis of the relationship:

$$\Delta G^{\circ} = -n\,F\,(E_m^{P/P+} - E_m^{Mn(II)/Mn(III)}) \quad (2.4)$$

where *n* is the number of electrons and *F* is the Faraday constant.[25] The parameter *B*, that is, the P^+ fraction remaining at high Mn-protein concentration determined for each reaction center mutant (Equation 2.3), was related to the difference in the midpoint potentials $E_m^{P/P+}$ and $E_m^{Mn(II)/Mn(III)}$:

$$B = C\left(1+e^{-\left(\left(E_m^{Mn(II)/Mn(III)}-E_m^{P/P+}\right)*(nF/RT)\right)}\right)^{-1}+D \quad (2.5)$$

where *R* is the gas constant, *T* is the temperature, which was 298 K, and *C* and *D* are the P^+ fractions reduced and remaining at high $E_m^{P/P+}$, where ΔG° is large. For the fits, the value of *n* was fixed to 1, and the sum of *C* and *D* was constrained to 1. The $E_m^{P/P+}$ values of the wild type and mutants were previously reported, corrected as needed using the dependence of –12 mV per pH value.[14,53]

Results

Reduction of P^+ by Mn-protein. In the presence of terbutryne, the light-minus-dark difference optical spectrum of the high-potential HHHH reaction centers shows spectral changes characteristic of the $P^+Q_A^-$ charge-separated state (Figure 2.4). A decrease, or bleaching, in the 865-nm absorption band indicates formation of oxidized primary donor, P^+. Electrochromic shifts in the 760 and 800-nm bands indicate the presence of reduced primary quinone, Q_A^-. The addition of Mn-protein to the reaction centers decreased the extent of bleaching of the 865-nm absorption band, and the electrochromic shifts in the 760 and 800-nm bands became more pronounced. As the concentration of the Mn-protein was increased from 0 to 17.5 μM, a larger loss of bleaching at 865 nm was observed, consistent with the transfer of an electron from the P1 Mn-protein to P^+.

The amount of the relative P^+ fraction was measured for different concentrations of Mn-protein (Figure 2.5). This dependence for the P1 Mn-protein and HHHH reaction centers at pH 9.4 was fit using Equation 2.3, yielding values of 1.2 ± 0.2 μM and 0.51 ± 0.02 for K_D and *B,* respectively (Table 2.1). Titrations with the P1-1 and P1-2 variants yielded slightly higher K_D values of 8.5 ± 1.3 μM and 8.0 ± 2.0 μM, respectively, but similar values of *B,* 0.45 ± 0.04 and 0.42 ± 0.05, respectively. Assuming that *B*, the limiting value for the relative P^+ fraction at high concentrations of the Mn-protein, is the same for all three Mn-proteins, the fits are not significantly changed (Figure A1). For example, constraining the *B* value to be the average of the three, 0.46, yielded in K_D values of 1.9 ± 0.2, 8.0 ± 0.3, and 6.7 ± 0.7 μM for the P1, P1-1, and P1-2 Mn-proteins, respectively (Table A1).

Dependence on P/P^+ midpoint potential. Light-minus-dark difference spectra were measured for reaction center mutants whose $E_m^{P/P+}$ values ranged from 468 to 748 mV in the absence and presence of the P1 Mn-protein at pH 9.4 (Figure 2.6). The amplitude of the spectral features decreases as the $E_m^{P/P+}$ increases as a result of changes in the forward electron transfer and charge recombination rates and the quantum yield of the initial electron transfer in the mutant reaction centers.[49] In general, the extent of change in the presence of the Mn-protein increased for reaction centers with larger $E_m^{P/P+}$ potentials. Addition of the P1 Mn-protein to the HFLF reaction center showed no measureable effect on the extent of bleaching compared to that in the absence of the Mn-protein, as was also observed for the wild-type reaction center, which has a $E_m^{P/P+}$ of 488 mV at pH 9.4. Increasing the $E_m^{P/P+}$ values, to 618, 693, and 748 mV in the HHHF, HHLH, and HHHH reaction centers, respectively, resulted in larger differences in the extent of bleaching upon addition of the P1 Mn-protein.

The relative P^+ fractions of reaction centers with different $E_m^{P/P+}$ values were monitored during titrations of the P1 Mn-protein at pH 9.4 and fit to Equation 2.3 for those mutants that showed a change in the relative P^+ fraction of >10% at high Mn-protein concentrations (Figure 2.7). The K_D values were very similar, ranging from 1.2 to 3.4 μM with an average error of ± 0.7 μM for the five variations of reaction centers (Table 2.1). The *B* value, corresponding to the relative P^+ fraction at high Mn-protein concentrations, decreased with increasing $E_m^{P/P+}$ values of the reaction centers. For example, the values of the *B* parameter for the HHHF (618 mV) and HHLH (693 mV) reaction centers were 0.78 ± 0.01 and 0.63 ± 0.01, respectively, compared to 0.51 ± 0.02

for the HHHH (748 mV) reaction centers. Using an assumption that the mutations that alter the midpoint potential do not change the binding, the data were also fit with the K_D value constrained to be the same average value of 2.0 μM for the fits of each of the reaction centers, yielding similar *B* values and a similar dependence on $E_m^{P/P+}$ (Figure A2, Table A2).

The effect of the P1 Mn-protein on the bleaching was observed only for reaction centers that contained the Leu L131 to His mutation, even for reaction centers with a relatively high P/P^+ midpoint potential. For example, the $E_m^{P/P+}$ of the LHHH reaction centers (683 mV) is similar to that of the HHLH reaction centers (693 mV); however, the addition of the Mn-protein did not alter the extent of bleaching for the LHHH reaction centers, while a measurable change was observed for the HHLH reaction centers (Figure 2.6). Because of the influence of the L131 mutation, the dependence on the $E_m^{P/P+}$ of the mutant reaction centers was analyzed only for those containing His L131.

The correspondence between the spectral changes and the reaction center mutants showed that the Mn-protein is more effective at reducing P^+ in reaction centers with higher $E_m^{P/P+}$ values (Table 2.1). The relationship between $E_m^{P/P+}$ and the parameter *B*, the relative P^+ fraction at high concentrations of the P1 Mn-protein, was analyzed using the Nernst equation (Equation 2.5). A *B* value of 1.0 was included for the HFLF (468 mV) and HHLF (568 mV) reaction centers. The data are described well with values of 633 ± 12 mV for $E_m^{Mn(II)/Mn(III)}$ and 0.54 ± 0.04 for *D*, the P^+ fraction remaining at high $E_m^{P/P+}$ (Figure 2.7).

Dependence on pH. To determine the pH dependence of the interaction of the P1 Mn-protein with the HHHH reaction centers, measurements were performed from pH 8.4 to 9.6. Addition of the P1 Mn-protein to HHHH reaction centers at pH 9.4 had a much larger impact on the extent of bleaching than at pH 8.4 (Figure 2.6). Titrations of the P1 Mn-protein with HHHH reaction centers over this pH range revealed the clear trend of smaller relative P^+ fractions, that is, a larger reduction of P^+ by the Mn-protein, at higher pH values (Figure 2.8). Using Equation 2.3, the data from the titrations were fitted and showed that the K_D increased slightly from 0.9 ± 0.3 μM to 5.2 ± 2.5 μM as the pH was decreased from pH 9.6 to 8.4. The parameter *B* increased substantially at lower pH values, ranging from 0.49 ± 0.03 at pH 9.6 to 0.89 ± 0.02 at pH 8.4. The change in the *B* value with pH was related to the change in the difference of the midpoint potentials, $E_m^{P/P+}$ and $E_m^{Mn(II)/Mn(III)}$ (Equation 2.5). A linear fit of the pH dependence of the $E_m^{Mn(II)/Mn(III)}$ values yielded a change of –56 mV per pH unit (Figure 2.8).

Kinetics of P^+ reduction. The decay of the P^+ signal at 865 nm after pulse illumination was measured by transient optical spectroscopy. In the absence of the P1 Mn-protein, the P^+ state of the HHHH reaction centers decayed as a single exponential with a time constant of ~30ms (Figure 2.9). This value is similar to the $P^+Q_A^-$ charge recombination time of 40 ms previously measured for the HHHH reactioncenters.[14] In the presence of the P1 Mn-protein, the decay became multiexponential and required fitting with at least three components with time constants ranging from approximately 10 to 1000 ms.

Discussion

Here, we present a detailed characterization of the P1 Mn-protein serving as a secondary electron donor to the reaction center, including the binding, energetics, and involvement of protons. In this process, the Mn-protein and reaction center form a complex in equilibrium, with illumination resulting in a charge-separated state, followed by the transfer of an electron from one of the Mn-cofactors to P^+ (Figure 2.10). The ability of the P1 Mn-protein to transfer an electron to P^+ was measured by the change in bleaching in light-minus-dark optical spectra. Our results are consistent with the relative P^+ fraction in the presence of the Mn-protein being dependent on the following four factors: the binding of the P1 Mn-protein, the free energy difference for the Mn-oxidation reaction, proton release during the Mn-oxidation reaction, and the rate of the Mn-oxidation reaction in comparison to the competing charge-recombination reaction.

Binding of P1 Mn-protein to the reaction center. In our structural model, the Mn-protein docks to the periplasmic surface of the reaction center (Figure 2.1). The periplasmic surface is the binding site for the natural secondary donor, cytochrome c_2, and has features that allow cytochromes from many different species to bind and transfer electrons to P^+. The K_D value of 1.2 μM for binding of the P1 Mn-protein to the reaction center is comparable to the values observed for cytochromes. For example, a variety of cytochromes, such as cytochrome c_2 from the closely-related bacterium *Rhodobacter capsulatus* and cytochrome *c* from horse heart, have been found to bind with K_D values of 0.4-6 μM,[54] while the K_D for the native cytochrome c_2 from *R. sphaeroides* has been measured at 0.3 μM.[50] Thus, the reaction center surface provides a favorable area for the

binding of both natural and artificial water-soluble proteins that can serve as secondary electron donors.

The specific interactions that drive the binding of cytochromes have been identified but are difficult to apply to the binding of the four-helix bundle, as evidenced by the impacts of changing the surface charges for the P1 Mn-protein and cytochromes. Alterations of charged residues on both cytochrome c_2 and the cytochrome-binding site of the reaction center resulted in a large range of K_D values, from 0.01 to 250 μM.[50,55] The correlation between the extent of the K_D changes and the location of the residues supports the concept that electrostatic interactions between Lys residues on cytochrome c_2 and acidic residues on the reaction center direct the initial docking of cytochrome c_2 from *R. sphaeroides*. After the initial docking, the cytochrome-reaction center complex undergoes an ensemble of configurations involving critical roles for other interactions such as hydrogen bonding and van der Waals interactions, until the precise orientation and positioning of the cytochrome in the active configuration is established.[41,51,56] Relatively small increases in the K_D values were measured when Lys residues were introduced on the surface of the P1 Mn-protein in the P1-1 and P1-2 Mn protein variants, suggesting a more minor role of salt bridges in the binding, which is likely dependent upon other interactions involving specific molecular arrangements of amino acid residues of the two proteins.

Free energy difference for P^+ reduction. Once the P1 Mn-protein binds and the complex is formed, the measured amount of the P^+ fraction is determined by the yield of electron transfer from Mn(II) to P^+, which is dependent upon the free energy difference

associated with this electron transfer, ΔG°. The value of ΔG° is directly proportional to the difference of the P/P^+ and Mn(II)/Mn(III) midpoint potentials (Equation 2.4). Reaction centers modified to have larger $E_m^{P/P+}$ values, and hence larger ΔG° values, showed a greater yield of electron transfer. The relative P^+ fraction systematically decreased in the presence of 17.5 μM P1 Mn-protein from 1.0 to 0.52 as the $E_m^{P/P+}$ increased from 468 to 748 mV, consistent with the predicted impact of ΔG° (Figure 2.7). The relationship between $E_m^{P/P+}$ and the parameter *B*, the relative P^+ fraction at high concentrations of the P1 Mn-protein, was analyzed using the Nernst equation (Equation 2.5), yielding a value of approximately 635 mV for $E_m^{Mn(II)/Mn(III)}$ at pH 9.4, a value that is in accord with the midpoint potentials of other Mn cofactors.

Mn-clusters of proteins exhibit a fair range of midpoint potentials, reflecting the influence of the protein environment on poising the potential. This effect is demonstrated with Mn superoxide dismutase, which catalyzes the conversion of superoxide into molecular oxygen and hydrogen peroxide and has a mononuclear Mn-cofactor coordinated by imidazole and carboxylate ligands.[57] During catalysis, the Mn-cofactor cycles between the Mn(II) and Mn(III) states with a midpoint potential ranging from 290 to 390 mV depending upon the conditions and source of enzyme. A Mn(II)/Mn(III) potential of >870 mV was observed when Mn replaced the Fe center of Fe-superoxide dismutase, whose metal-binding site is very similar to Mn-superoxide dismutase. In this case, the redox tuning effect of the protein environment is thought to be influenced by hydrogen bonding of the metal ligands with the surrounding protein environment. The role of metal ligands in establishing the potential has also been well investigated using

synthetic compounds that mimic features of Mn enzymes and exhibit many different potentials. For example, synthetic mononuclear Mn(II) complexes have potentials ranging from –1100 to +800 mV.[58–62]

A mononuclear Mn binding site has previously been introduced into highly oxidizing reaction centers in a position comparable to that of the Mn_4CaO_5 cluster of photosystem II. Upon illumination of these reaction centers, with an $E_m^{P/P+}$ of 760 mV at pH 8, P^+ is rapidly reduced by the Mn-cofactor, which has an $E_m^{Mn(II)/Mn(III)}$ of 625 mV at pH 9, similar to the value for the P1 Mn-protein.[24,25] For the mononuclear Mn cofactor, the potential is significantly decreased to 535 mV in the presence of bicarbonate, which acts as a synergistic anion and likely provides additional ligands into the relatively open binding site. Synergistic anions facilitate the binding of Mn and Fe to proteins and have a pronounced impact on the electronic structure of the metal, including the potential.[63,64] Compared to the mono-nuclear binding site, the dinuclear Mn-binding sites in the P1 Mn-protein are more encased by the hydrophobic core of the four-helix bundle and include a carboxylate bridge between the metals. These results demonstrate the impact of the Mn environments on potential and hence the opportunity to manipulate the electronic structure of the Mn in the design of artificial Mn-proteins.

Proton release upon Mn oxidation. The coupling of proton and electron transfer is common in redox-active proteins, as the release of the proton upon metal oxidation, and uptake of protons upon cofactor reduction, is often required to maintain an overall charge neutrality.[65] The role of protons in the Mn oxidation reaction was probed by measuring the pH dependence of electron transfer from the P1 Mn-protein to the HHHH reaction

centers between pH 9.6 and 8.4 (Figure 2.8). While the binding of the Mn-protein was only weakly dependent on pH, the extent of P^+ reduction at high Mn-protein concentrations showed a significant dependence on pH. The pH dependence of the extent of reduction was related to a change in the midpoint potential of the Mn cofactor, $E_m^{Mn(II)/Mn(III)}$ of –56 mV/pH (Figure 2.8). This slope corresponds to one proton being released upon Mn oxidation. A similar pH dependence is observed for the midpoint potentials of cofactors of other proteins, such as the redox-active tyrosine Y_Z of photosystem II, which is involved in the coupling of proton transfer to electron transfer in water oxidation.[66] These pH dependencies reflect the coupling of protons with electrons, which is critical in achieving multi-step electron transfer as performed by Mn-proteins such as photosystem II.[67]

The transfer of an electron from the Mn-cluster to P^+ appears to be also limited by a factor associated with Leu L131, which is immediately adjacent to P (Figure 2.2), as this electron transfer step was only observed in reaction centers with the change to His L131. For example, the extent of bleaching did not change upon addition of the P1 Mn-protein to the LHHH reaction centers even though they have a relatively high $E_m^{P/P+}$ value of 683 mV (Figure 2.6). The L131 mutation has been previously shown to result in changes in a number of properties of the dimer, in particular loss of proton release upon formation of P^+.[68,69] While flash illumination results in limited proton release, as the associated rate is relatively slow,[70,71] illumination lasting several minutes results in release of a large number of protons per reaction center for wild type. However, only a small amount is released for HHLF reaction centers. The proton transfer chain is thought to involve a

number of protonatable side chains as well as water molecules, with the Leu to His alteration of L131 disrupting the proton chain by repositioning nearby Tyr M210.[69] Under the conditions used for the light-minus-dark measurements for the Mn-protein and reaction centers reported in this paper, it is likely that the His L131 mutation inhibits proton release due to formation of P^+. Consequently, a proton would be available that could be coupled with the reduction of P^+ by the Mn-protein. However, in wild type and reaction centers with Leu L131, because formation of the $P^+Q_A^-$ charge separated state results in proton release, the lack of the proton near P^+ would restrict reduction by the Mn cluster.

Competition of electron transfer rates. The yield of electron transfer from the P1 Mn-protein to P^+ was less than unity, even at relatively high Mn-protein concentrations for reaction centers with high P/P^+ midpoint potentials at high pH, indicating that another factor played a role in addition to the binding, free energy difference, and proton release. For example, the $E_m^{P/P+}$ value of 748 mV for HHHH reaction centers is significantly above the observed $E_m^{Mn(II)/Mn(III)}$ and corresponds to a value of –110 meV for $\Delta G°$ (Equation 2.4). The yield of Mn-oxidation for these reaction centers was approximately 50%, as signified by the parameter *D* in Equation 2.5, indicating that P^+ reduction is limited by an aspect other than the free energy difference. It is likely that the yield of formation of the P1Mn(III):PQ_A^- state is reduced because of competition between charge recombination from the P1Mn(II):$P^+Q_A^-$ state to the ground state and transfer of an electron from the P1 Mn-cofactor to P^+. After absorption of light by the HHHH reaction centers, the charge-separated $P^+Q_A^-$ state decayed to the ground state by charge

recombination with a time constant of ~31 ms (Figure 2.9), which is faster than the time of 100 ms for wild-type reaction centers due to the increase in the free energy difference for charge recombination in the HHHH reaction centers.[72] In the presence of the P1 Mn-protein, the recovery of the P^+ state of the HHHH reaction centers was measured to contain multiple decay components, with time constants comparable to the time constant of charge recombination. The complexity of the decay probably reflects differences in the rates of transfer from each of the three metal centers of the P1 Mn-protein to P^+. In contrast, P^+ was fully reduced by a mononuclear Mn bound to the highly oxidizing reaction center with a first-order rate having a lifetime of 12 ms.[24] These results with the bound Mn-cofactor indicate that the design of Mn-cofactors in artificial domains that are fused to the reaction center promises to create a complex that will completely reduce P^+ as a first-order reaction.

Summary. The P1 Mn-protein can bind to reaction centers and reduce P^+ after illumination, consistent with a model of the P1 Mn-protein docking to the periplasmic surface of the reaction center and serving as a secondary electron donor. Consideration of an overall scheme allowed delineation of the impact of different factors on the yield of electron transfer (Figure 2.10). Although the P1 Mn-protein is an artificial protein, the accommodating periplasmic surface of the reaction center provides sufficient interactions for binding, just as it allows a range of cytochromes to serve as secondary donors. The results identify the conditions under which the Mn-protein is maximally associated with the reaction center, the free energy difference for the reaction is large, and protons can be released. The Mn-protein is water-soluble and binds only transiently to the reaction

center, and hence transfers only one electron as a second-order process. A major improvement in the efficiency of the electron transfer would be in incorporation of the Mn-protein as a covalently bound domain, as the electron transfer process would change from a second-order to a first-order process, the efficiency of electron transfer should improve, and the fusion complex should be capable of multi-electron transfer processes. In addition, a fused Mn domain would open a rich environment for the addition of non-native cofactors to the bacterial reaction center to drive novel oxidation-reduction reactions.

Acknowledgments

We thank Dr. Marco Flores for usage of the laser system for the transient optical measurements.

Figures

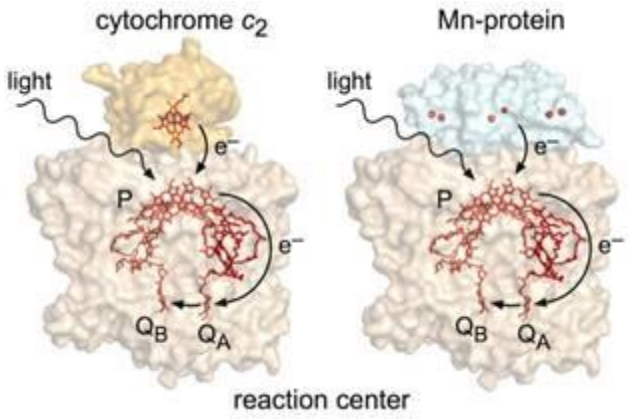

Figure 2.1. Models of electron transfer from cytochrome c_2 (left) and the Mn-protein (right) to the reaction center. Docking of either the cytochrome c_2 (orange) or Mn-protein (light blue) to the periplasmic surface of the reaction center (wheat), brings the heme (red) or dinuclear Mn-clusters (red), respectively, into the proximity of the reaction center cofactors (red). Upon illumination of the bacteriochlorophyll dimer, an electron is transferred along the active branch of cofactors, and the docked protein can act as a secondary electron donor, reducing the oxidized bacteriochlorophyll dimer. Shown are the L and M subunits of the reaction center, with the H subunit is not shown for the sake of simplicity.

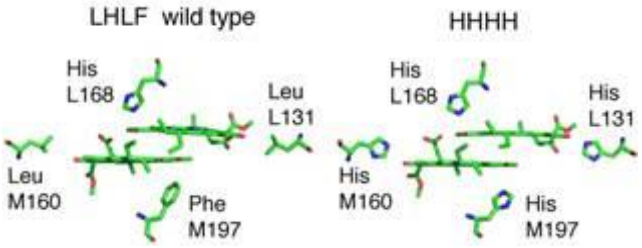

Figure 2.2. Structures of the bacteriochlorophyll dimer, P, in LHLF (wild-type) and HHHH reaction centers showing the amino acid residues L131, L168, M160, and M197 (colored by atom type). At each of these positions, residues that form hydrogen bonds to the conjugated system increase the P/P^+ midpoint potential, $E_m^{P/P+}$.[14,44] A hydrogen bond with His results in increases in $E_m^{P/P+}$ of 60–125 mV, with smaller increases seen for hydrogen bonds with Glu and Asp. The changes in $E_m^{P/P+}$ are additive for each mutation, so that the $E_m^{P/P+}$ for HHHH reaction centers, with four hydrogen bonds, is 260 mV higher than that of wild-type LHLF reaction centers, which have one hydrogen bond. A range of 355 mV in $E_m^{P/P+}$ can be attained with different combinations of mutations in the reaction centers.

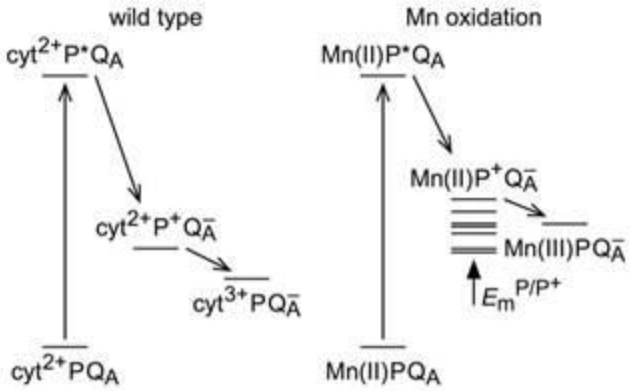

Figure 2.3. Energy-level diagrams for the light-induced formation of charge-separated states. In reaction centers, absorption of light results excitation of the bacteriochlorophyll dimer, P, followed by electron transfer to produce the oxidized P^+ and reduced quinone Q_A^-, when electron transfer to the secondary quinone is blocked. In wild type, P^+ is subsequently reduced by cytochrome c_2 (left). Reaction centers with different P/P^+ midpoint potentials ($E_m^{P/P+}$) have correspondingly altered energies of the charge-separated states involving P^+. Because the Mn(II)/Mn(III) midpoint potential is higher than the cytochrome c_2^{2+}/cytochrome c_2^{3+} midpoint potential, the P/P^+ midpoint potential must be higher than in the wild type for the reaction centers to be capable of oxidizing Mn(II).

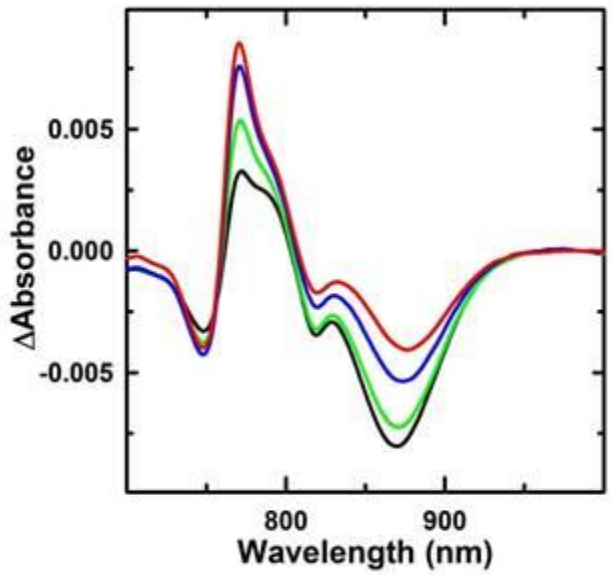

Figure 2.4. Addition of the P1 Mn-protein to HHHH reaction centers. Shown are light-minus-dark optical spectra of HHHH reaction centers in the presence of terbutryne without the P1 Mn-protein (black), and in the presence of 0.5 μM (green), 2.5 μM (blue) and 17.5 μM (red) P1 Mn-protein. The assay starting condition included 1.5 μM HHHH reaction centers in 15 mM CHES (pH 9.4), 0.03 % Triton X-100 and 100 μM terbutryne.

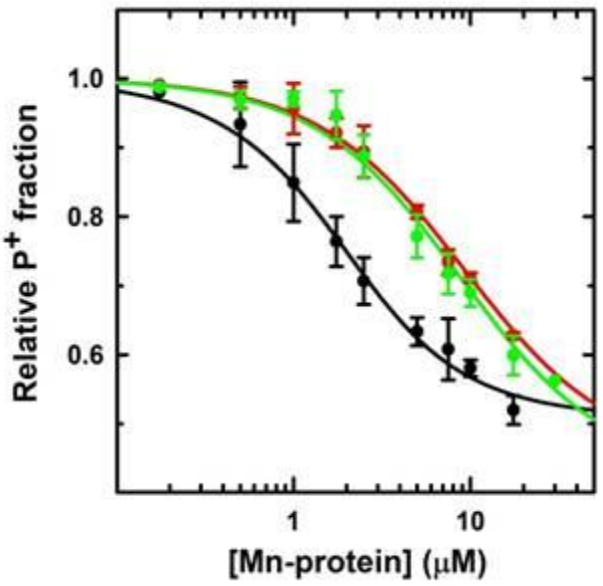

Figure 2.5. Titrations of HHHH reaction centers with the P1 (black), P1-1 (red), and P1-2 (green) Mn-proteins. The P1-1 and P1-2 Mn-proteins have altered surface residues compared to those of the P1 Mn-protein. For each Mn-protein, the data from three titrations were averaged and fit to Equation 2.3, yielding the dissociation constant, K_D, and the relative P^+ fraction at high Mn-protein concentrations, *B*. For the P1, P1-1, and P1-2 Mn-proteins, the values of K_D obtained from the fits were 1.2, 8.5, and 8.0 μM, and the values of *B* were 0.51, 0.45, and 0.42, respectively (Table 2.1).

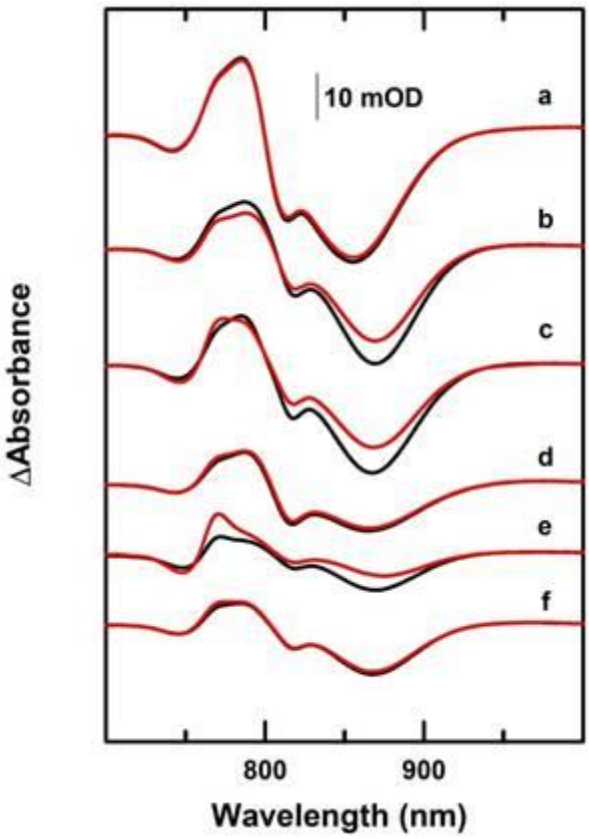

Figure 2.6. Light-minus-dark optical spectra of reaction centers without (black) and with (red) 5 μM P1 Mn-protein for reaction centers with substitutions that alter the P/P^+ midpoint potential, $E_m^{P/P+}$, and at two pH values: (a) HFLF reaction centers ($E_m^{P/P+}$ = 468 mV) at pH 9.4, (b) HHHF reaction centers ($E_m^{P/P+}$ = 618 mV) at pH 9.4, (c) HHLH reaction centers ($E_m^{P/P+}$ = 693 mV) at pH 9.4, (d) LHHH reaction centers ($E_m^{P/P+}$ = 683 mV) at pH 9.4, (e) HHHH reaction centers ($E_m^{P/P+}$ = 748 mV) at pH 9.4, and (f) HHHH reaction centers ($E_m^{P/P+}$ = 760 mV) at pH 8.4. The reaction centers were at a concentration of 1.5 μM in 15 mM CHES (pH 9.4) or Tris-HCl (pH 8.4), 0.03 % Triton X-100, and 100 μM terbutryne.

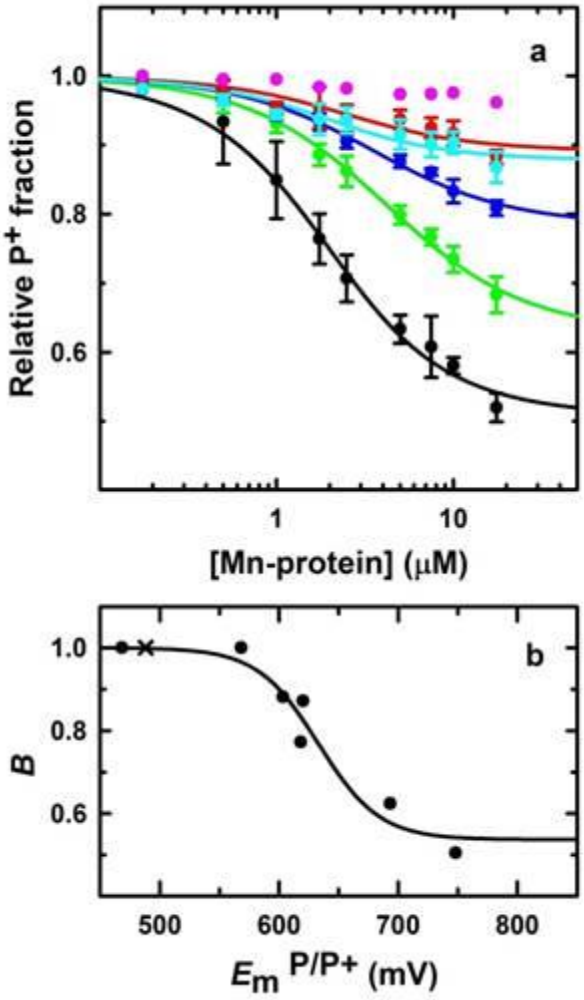

Figure 2.7. (a) Titrations of reaction centers having different P/P^+ midpoint potentials with the P1 Mn-protein. Shown are HFLF (pink), HHDF (red), HHHF (blue), HHEF (cyan), HHLH (green) and HHHH (black) reaction centers, with $E_m^{P/P+}$ values of 468, 603, 618, 620, 693, and 748 mV, respectively. Each of the reaction centers in this set contains the Leu L131 to His mutation. The decrease in the relative P^+ fraction was greater in reaction centers with a higher $E_m^{P/P+}$. The *B* values, which signify the P^+ fraction at excess P1 Mn-protein, were correlated with the $E_m^{P/P+}$ values, while the K_D values from fits to the average of three titrations to Equation 2.3 were similar (Table 2.1). (b) Dependence of *B* on the $E_m^{P/P+}$ value of the reaction center (filled circles), compared to wild type (x). The best fit to Equation 2.5 (solid line) yielded values of 633 ± 12 mV for $E_m^{Mn(II)/Mn(III)}$ and 0.54 ± 0.04 for *D*, which is the P^+ fraction remaining at high $E_m^{P/P+}$.

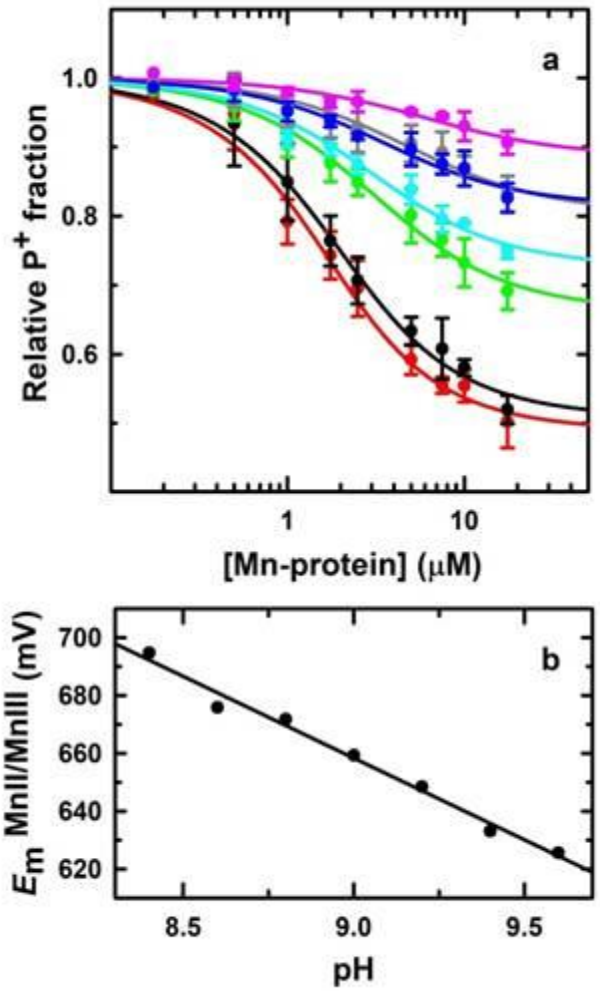

Figure 2.8. (a) Titrations of HHHH reaction centers with the P1 Mn-protein under conditions that span a range of pH values. The average data from three titrations at pH values of pH 8.4 (pink), pH 8.6 (blue), pH 8.8 (gray), pH 9.0 (cyan), pH 9.2 (green), pH 9.4 (black) and pH 9.6 (red) are shown. The decrease in the relative P^+ fraction is greater at higher pH values. The dissociation constants obtained from fits of the average of three titrations to Equation 2.3 showed a slight increase with a decrease in pH, and the limiting values for the relative P^+ fraction at high concentrations of the Mn-protein showed a significant increase with a decrease in pH (Table 2.1). (b) pH dependence of the Mn(II)/Mn(III) midpoint potential, $E_m^{Mn(II)/Mn(III)}$, of the Mn cofactors of the P1 Mn-protein. A linear best fit yields $E_m^{Mn(II)/Mn(III)}$ decreasing at higher pH values with a slope of –56 ± 3 mV per pH unit (solid line).

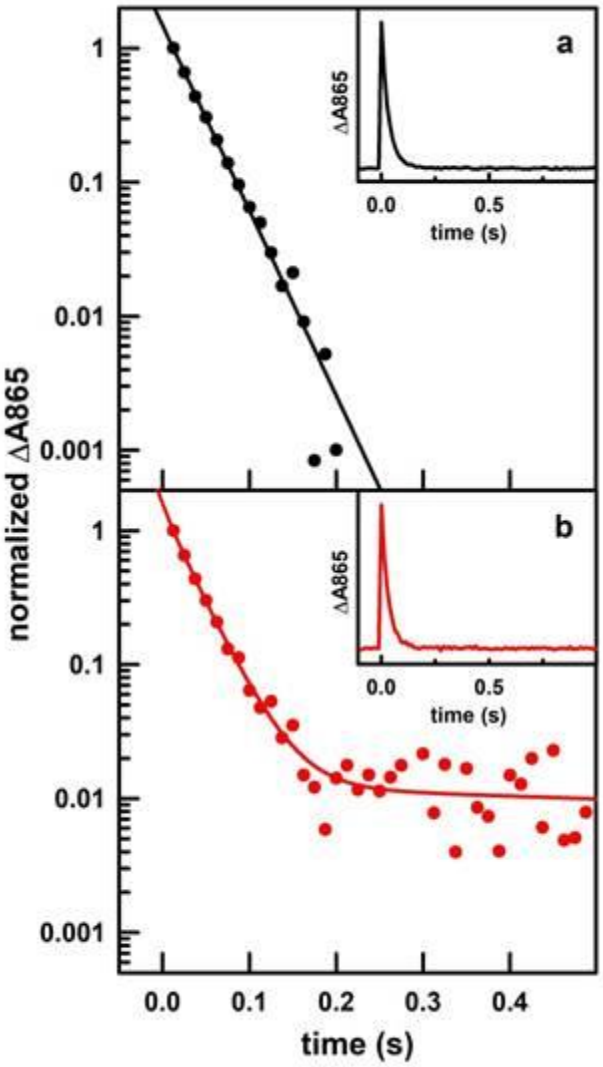

Figure 2.9. Kinetics of P^+ decay measured at 865 nm in the HHHH reaction centers. (a) In the absence of the P1 Mn-protein, the decay is described well by a single-exponential term with a time constant of 31 ms (black data and line). (b) In the presence of the P1 Mn-protein, fitting the decay requires at least three components, with a three-component best fit yielding time constants of 12, 32, and 2000 ms (red data and line). The reaction centers were at a concentration of 1.5 μM in 15 mM CHES (pH 9.4), 0.03 % Triton X-100 and 100 μM terbutryne.

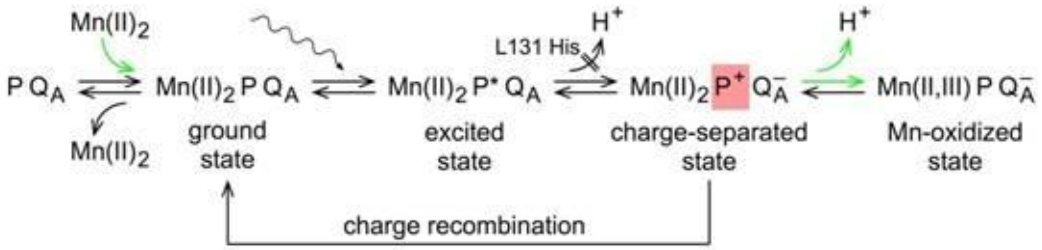

Figure 2.10. Scheme showing the steps in the binding and electron transfer of the P1 Mn-protein containing a $Mn(II)_2$ cofactor to the reaction center, represented by the primary electron donor P, which is a bacteriochlorophyll dimer, and the primary electron acceptor Q_A, which is a quinone. In the reaction center, light excitation of P is followed by charge separation, and the amplitude of the P^+ component (shaded red) was measured in the light-minus-dark spectra. In three of the steps (green arrows), the conditions were manipulated to maximize the production of the Mn-oxidized state, that is, by increasing the amount of the Mn-protein, by increasing the free energy difference for the Mn(II) to P^+ electron transfer step, and by increasing the pH of the reaction. The L131 Leu to His mutation blocks proton release upon formation of the charge-separated state, allowing proton release that is proposed to be required for formation of the Mn-oxidized state. Competition from the charge recombination reaction results in a decrease in the yield of formation of the Mn-oxidized state.

Tables

Table 2.1. Dissociation constants and extents of bleaching at high Mn-protein concentrations obtained from fits of titrations of reaction centers with Mn-proteins.[a]

Mn-protein	Reaction Center[b]	$E_m^{P/P+}$ (mV)[c]	pH	K_D (μM)	B
P1	wild type/LHLF	488	9.4	–	–
P1	HHHH	748	9.4	1.2 ± 0.2	0.51 ± 0.02
P1-1	HHHH	748	9.4	8.5 ± 1.3	0.45 ± 0.04
P1-2	HHHH	748	9.4	8.0 ± 2.0	0.42 ± 0.05
P1	HHLH	693	9.4	3.4 ± 0.5	0.63 ± 0.01
P1	LHHH	683	9.4	–	–
P1	HHEF	620	9.4	1.1 ± 0.9	0.88 ± 0.02
P1	HHHF	618	9.4	2.8 ± 0.6	0.78 ± 0.01
P1	HHDF	603	9.4	1.7 ± 1.3	0.89 ± 0.02
P1	HHLF	568	9.4	–	–
P1	HFLF	468	9.4	–	–
P1	HHHH	746	9.6	0.9 ± 0.3	0.49 ± 0.03
P1	HHHH	751	9.2	2.3 ± 0.6	0.66 ± 0.02
P1	HHHH	753	9.0	2.2 ± 0.6	0.73 ± 0.02
P1	HHHH	755	8.8	4.0 ± 1.4	0.80 ± 0.02
P1	HHHH	758	8.6	2.7 ± 1.0	0.81 ± 0.02
P1	HHHH	760	8.4	5.2 ± 2.5	0.89 ± 0.02

[a]The data in Figures 2.5, 2.7, and 2.8 were fit to Equation 2.3.

[b]The amino acid residues in wild-type reaction centers are Leu L131, His L168, Leu M160, and Phe M197, designated in order as LHLF. The other strains have combinations

of mutated residues His L131, Phe L168, His M160, Glu M160, Asp M160, and His M197.

[c]The P/P^+ midpoint potentials of the reaction centers were measured at pH 8.0 and have been adjusted to pH 9.4 by –12 mV/pH unit.[14,44,53]

CHAPTER 3

ELECTRON TRANSFER FROM A SUITE OF FOUR-HELIX MN-PROTEINS AND A FOUR-HELIX FE-PROTEIN TO MODIFIED REACTION CENTERS

Abstract

Four-helix bundles with binding sites for di-nuclear metal clusters are useful for incorporating metal cofactors. In this study we use a variety of such proteins, designated P, to characterize electron transfer to reaction centers from *Rhodobacter sphaeroides*. Light-minus-dark optical measurements show that the P Mn-proteins and P1 Fe-protein can act as secondary donors to reaction centers. The dissociation constants of the P Mn-proteins are similar, with an average dissociation constant of 2.3 μM. The activity of the P Mn-proteins is dependent on the number of di-nuclear binding sites present in the protein design. The P Mn-proteins with three di-nuclear binding sites affect the reaction centers to a greater extent than those with one di-nuclear binding site. The P1 Fe-protein shows a decrease in the reaction center bleaching, indicating that it was a secondary electron donor. However, measurement of the activity is inconsistent. My interpretation is that the high pH value of 9.4 used in the measurements caused oxidation of the P1 Fe-protein. In conclusion, the P Mn-proteins and P1 Fe-protein are capable of electron transfer to reaction centers. The measurements with the P1 Fe-protein is inconsistent over time, making it difficult to characterize the electron transfer to reaction centers.

Introduction

The goal of the work described in this chapter is to characterize the reduction-oxidation reactions of di-nuclear manganese cofactors with the oxidized bacteriochlorophyll dimer (P^+), the primary electron donor in bacterial reaction centers

from *Rhodobacter sphaeroides*. The artificial four-helix P proteins are used because of the interesting design feature of binding di-nuclear cofactors. The design of the artificial four-helix P proteins is inspired by the work from DeGrado and coworkers[32] on the *due ferri* (DF) proteins that bind di-nuclear Fe cofactors. The artificial P proteins are viable secondary electron donors to bacterial reaction centers through a one-electron reduction-oxidation reaction as shown in Chapter 2. In this chapter, I continue to build on my work with artificial P proteins by characterizing the binding to bacterial reaction centers of a suite of P Mn-proteins: P0, P1, P2 and P3. The P1 Fe-protein binds and reduces bacterial reaction centers albeit with some challenges.

The binding of the P1 Mn-protein to bacterial reaction centers is described as being similar to cytochrome c_2 binding to bacterial reaction centers.[46] The primary interaction in the binding of cytochrome c_2 and bacterial reaction centers is surface-based electrostatic interactions.[40] A co-crystal structure of cytochrome c_2 and bacterial reaction centers reveals that the periplasmic surface of bacterial reaction centers is negatively charged, and that cytochrome c_2 is positively charged surface, particularly the surface of the protein that interacts with the bacterial reaction centers.[41] In HHHH reaction centers, the bacterial reaction centers surface is unchanged in comparison to the wild-type reaction center, so proteins that behave as secondary donors should depend on electrostatic interactions to bind to bacterial reaction centers.

One-electron reduction-oxidation reactions are dependent on the difference in free energy of the reaction with lower free energy states being more favorable in the reaction process. The HHHH reaction centers used in the experiments in this chapter have a P/P^+

mid-point potential that is greater than the wild-type reaction center by 260 mV.[14] Electron transfer from metals to bacterial reaction centers that lack a metal-binding site is a second-order process with metals binding transiently to the reaction centers.[16] Both Mn(II) and Fe(II) are secondary donors to bacterial reaction centers.[26] Mn(II) and Fe(II) have different effects on bacterial reaction centers making them interesting for binding to the artificial P proteins.

In this study I focus on the P0, P2, P1 and P3 Mn-proteins, which have one, two, three and three di-nuclear cofactors incorporated, respectively.[47] The electron transfer from the P Mn-proteins to P^+ is dependent on the number of di-nuclear cofactors. I also attempt to characterize electron transfer from the P1 Fe-protein to the HHHH reaction center. The reaction is possible, but inconsistent because the activity varies over time, making it difficult to characterize. My interpretation is that the pH of the assay affected the extent of the activity of the P1 Fe-protein.

Materials and Methods

Preparation of reaction centers from *Rhodobacter sphaeroides*. The reaction center isolation was previously described.[24] In this study the highly oxidizing HHHH reaction center was used to characterize electron transfer from the P Mn-proteins and P1 Fe-protein. The HHHH reaction center has been previously described in Chapter 2 of this dissertation and in other articles.[14] The HHHH reaction center was stored at –80°C with the following buffer conditions: 15 mM Tris-Cl (pH 8.0) and 0.05 % Triton X-100. The titration experiments with P proteins were done at pH 9.4. Prior to use, the reaction centers were exchanged into 15 mM CHES (pH 9.4), 0.025 % Triton X-100 through a 50-

fold dilution and concentration using an Amicon filter with a 30000 Da molecular weight cut-off (MWCO).

Preparation of P proteins from *Escherichia coli*. The description of the P0, P1, P2 and P3 protein design was reported in a previous article.[47] The description of P protein isolation from *Escherichia coli* was described in Chapter 2. The P proteins were all stored at –80°C in ultra-pure water. The addition of Mn and Fe to P proteins was all done in ultra-pure water prior to titrations with HHHH reaction centers at pH 9.4.

Description of light-minus-dark optical spectroscopy on HHHH reaction centers. Light-minus-dark optical changes were measured using a Varian Cary 6000i ultraviolet-visible-near IR spectrometer (Agilent Technologies). The HHHH reaction centers were illuminated using sub-saturating light from a 1000 W tungsten bulb with an 860 nm filter as previously described.[24]

Dissociation constants determined from the P Mn-protein titrations, K_D. The binding of Mn to the apo P proteins followed procedures that were previously described in Chapter 2. Final concentrations of the P Mn-proteins ranged from 350–600 μM. The P0 Mn-protein was a special case from P1, P2 and P3 Mn-proteins because the P0 Mn-protein concentration was limited by the protein solubility. The final P0 Mn-protein concentration ranged from values of 100–150 μM.

The starting reaction center concentration for each P Mn-protein experiment was 1.5 μM of the HHHH reaction centers in 15 mM CHES (pH 9.4), 0.03 % Triton X-100 and 100 μM terbutryne with a final volume of 750 μL. The concentration of the P Mn-protein was incrementally raised through values ranging from 0.175–17.5 μM. The light-minus-

dark optical measurements were made for HHHH reaction centers without the P Mn-protein. Additionally, the light-minus-dark optical measurements were made at a range of P Mn-protein concentrations. A full description of the measurement was described in Chapter 2. Additionally, the analysis of the data was similar to the description provided in Chapter 2. The relative P^+ fraction was determined using Equation 2.2 from Chapter 2. To determine the dissociation constant (K_D), Equation 2.3 from Chapter 2 was used to fit the titration data.

Relative P^+ decrease in HHHH reaction centers with P1 Fe-protein. The apo-P1 protein in ultra-pure water at a concentration of 75 μM was mixed with 450 μM ferrous sulfate with a final volume of 1 mL in a glove box (MBraun Lab Master 130). The mixture was incubated in the glove box for five minutes giving time for Fe incorporation to the apo-P1 protein binding sites. To remove free Fe from the mixture, dialysis against 300-mL of ultra-pure water was done for 30 minutes. The water for dialysis was degassed using an aspirator. The P1 Fe-protein mixture was put in dialysis tubing with a 1000 Da MWCO. Immediately following dialysis the reaction centers were mixed with the P1 Fe-protein.

The P1 Fe-protein experiments with HHHH reaction centers were done by comparing samples of HHHH reaction centers with and without the P1 Fe-protein. The starting conditions of the HHHH reaction centers without the P1 Fe-protein were 1.0 μM reaction centers in 15 mM CHES (pH 9.4), 0.03 % Triton X-100 and 100 μM terbutryne. The starting conditions of the HHHH reaction centers with P1 Fe-protein were 1.0 μM HHHH reaction centers in 15 mM CHES pH 9.4, 0.03 % Triton X-100, 100 μM terbutryne and

50 μM P1 Fe-protein. To evaluate the decrease of P^+ with P1 Fe-protein, the change in absorption at 865 nm with metal (ΔA^{M}_{865}) and the change in absorption at 865 without the metal (ΔA^{0}_{865}) were used to calculate the relative P^+ decrease:

$$\text{relative } P^{+}\text{decrease} = \frac{\Delta A^{M}_{865}}{\Delta A^{0}_{865}} \quad (3.1)$$

The P1 Fe-protein experiments were repeated for multiple trials for several months to establish the consistency of the reaction.

Results

This section will cover the results obtained by adding P Mn-proteins and P1 Fe-protein to HHHH reaction centers at pH 9.4. Electron transfer is observed in both cases where Mn and Fe are bound to the P proteins. Comparison of the effect of the P0, P1, P2 and P3 Mn-proteins on the relative P^+ fraction is correlated to the number of di-nuclear binding sites. The P1 Fe-protein electron transfer to the HHHH reaction centers is inconsistent making it difficult to characterize the electron transfer reaction.

P Mn-proteins electron transfer to HHHH reaction centers. The light-minus-dark optical changes of HHHH reaction centers in the presence of terbutryne and without Mn-proteins shows a decrease in absorption centered at 865 nm and an increase in absorption centered at 770 nm (Figure 3.1). The optical changes in HHHH reaction centers without P Mn-proteins are consistent with steady-state formation of the charge-separated state, $P^+Q_A^-$. The decrease centered at 865 nm indicates a loss of P upon illumination and the increase centered at 770 nm results from electrochromic shifts of the bacteriochlorophyll and bacteripheophytin absorption bands. When P0, P1, P2 and P3 Mn-proteins are added to HHHH reaction centers and terbutryne, the effect is a decrease in the bleaching of the

band centered at 865 nm. Moreover, we observe a relative increase in absorption centered at 770 nm compared to HHHH reaction centers without P proteins. In this chapter, HHHH reaction centers without Mn-protein and with 17.5 μM P2 and P3 Mn-protein are shown as representative data (Figure 3.1). A relative decrease in the extent of bleaching at 865 nm and a positive increase at 770 nm indicates electron transfer from the P Mn-protein to HHHH bacterial reaction centers. The decrease in the extent of bleaching in HHHH reaction centers and terbutryne is more pronounced in P proteins with larger number of di-nuclear cofactors. In Figure 3.1 the HHHH reaction centers bleach less when mixed with P3 Mn-protein than P2 Mn-protein at 17.5 μM.

The change in absorption at 865 nm from light-minus-dark data of HHHH reaction centers and terburyne with and without Mn-protein are used to determine the relative P^+ fraction using Equation 2.2. The relative P^+ fraction was plotted against the Mn-protein concentration, and the data were fit to Equation 2.3, presented Chapter 2, to determine the dissociation constant (K_D) (Figure 3.2). The K_D values obtained from the fits are 1.6 ± 3.8, 1.7 ± 0.4, 3.4 ± 0.8 and 2.4 ± 0.5 μM for P0, P1, P2 and P3, respectively. The relative P^+ fraction values at 17.5 μM for P0, P1, P2 and P3 Mn-proteins are 0.86 ± 0.04, 0.56 ± 0.01, 0.68 ± 0.04 and 0.53 ± 0.03, respectively. The values presented are an average of three separate titrations done for each Mn-protein. These values are useful for making comparisons of the effects of the protein on electron transfer reaction. The P0 Mn-protein has the largest value meaning less effect on the relative P^+ fraction, and the P3 Mn-protein has the lowest value meaning more effect on relative P^+ fraction.

P1 Fe-protein shows inconsistent electron transfer to HHHH reaction centers. The light-minus-dark optical changes of HHHH reaction centers without P1 Fe-protein show a decrease in absorption at 865 nm and an increase in absorption at 770 nm (Figure 3.3). This is a typical light-minus-dark spectrum as described previously. Addition of 50 μM P1 Fe-protein to HHHH reaction centers decreases the extent of bleaching and shows an increase at 770 nm, which is consistent with electron transfer to bacterial reaction centers (Figure 3.3). The data of P1 Fe-protein added to HHHH bacterial reaction centers vary in the relative P^+ decrease over time as shown in Table 3.1. The characterization of the P1 Fe-protein reaction is limited because of the standard deviation of 0.25 with my criteria being a standard deviation of 0.10.

Discussion

This section will cover findings, such as correlation of the decrease in relative P^+ fraction in HHHH reaction centers to the different number of cofactors in each P Mn-protein. Additionally, this section will cover the relative P^+ decrease in HHHH reaction centers mixed with P1 Fe-protein with a focus on the inconsistency of activity and the interpretation of the inconsistency in the measurements of electron transfer from the P1 Fe-protein to HHHH reaction centers.

P0, P1, P2 and P3 Mn-protein titrations to HHHH reaction centers. The average K_D value of the suite of Mn-proteins is 2.3 ± 0.8 μM, and my interpretation of the results is that the suite of Mn-proteins binds to HHHH reaction centers with a similar interaction. The largest standard deviation of the relative P^+ fraction values is 0.04, so the difference in values between P0, P1, P2 and P3 Mn-proteins suggests that the effect on the relative

P^+ fraction is correlated to the number of di-nuclear manganese cofactors. The P0 Mn-protein had a relative P^+ fraction value of 0.86 ± 0.04 at 17.5 μM Mn-protein, which is the largest relative P^+ fraction value. The P0 Mn-protein has one di-nuclear binding site, so the presence of one di-nuclear cofactor appears to be limiting the decrease in relative P^+ fraction. The P1 and P3 Mn-proteins have the lowest relative P^+ fraction values, and the values are similar to each other with 0.56 ± 0.01 and 0.53 ± 0.03 for P1 and P3 Mn-proteins, respectively. The similarity in the values of P1 and P3 Mn-proteins suggests that the presence of three di-nuclear cofactors increases the extent of the reaction. The P2 Mn-protein has a value that is between the P0 Mn-protein and the P1 Mn-protein, so the P2 protein is better at affecting the relative P^+ fraction in HHHH reaction centers than the P0 Mn-protein but not the P1 Mn-protein. In short, the different Mn-protein designs enable us to control the extent of the reaction.

Electron-transfer from the P1 Fe-protein to HHHH reaction centers. The P proteins are versatile in the metals that are possible to incorporate.[73] The P1 Fe-protein impacts the relative P^+ decrease. The effects of the P1 Fe-protein are inconsistent over time, with attempts over several months to make the reaction consistent. In Table 3.1, I present a representative data set of the relative P^+ decrease on HHHH reaction centers with the P1 Fe-protein. The standard deviation of the measurements was ±0.25, a value that is too large to have confidence in the effectiveness of P1 Fe-protein as a secondary electron donor. The stability of ferrous ions is strongly pH dependent with a tendency to oxidize spontaneously at high pH values. My conclusion is that ferrous ions in the P1 Fe-protein are spontaneously oxidized at pH 9.4. Presumably the di-nuclear cluster exposure

to the medium is significant enough to drive the spontaneous oxidation of the ferrous ions.

Figures

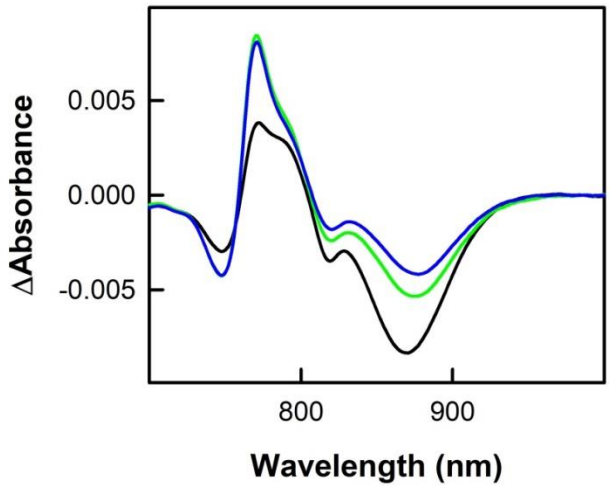

Figure 3.1. Light-minus-dark spectra of HHHH reaction centers with and without Mn-protein. The HHHH reaction centers and terbutryne without a P Mn-protein (black trace), with 17.5 μM P2 Mn-protein (green trace) and with 17.5 μM P3 Mn-protein (blue trace) show the extent of bleaching based on different Mn-proteins. The optical changes of reaction centers and terbutryne without a Mn-protein show the full extent of bleaching at 865 nm and a positive increase in absorption at 770 nm consistent with the $P^{+}Q_{A}^{-}$ state. Addition of the P2 Mn-protein (green trace) and P3 Mn-protein (blue trace) affect the decrease in extent of bleaching at 865 nm and show an increase in absorption at 770 nm. The result is consistent with electron transfer from the Mn-protein to the reaction centers. The assay conditions were the following: 1.5 μM HHHH reaction centers in 15 mM CHES (pH 9.4), 0.03 % Triton X-100 and 100 μM terbutryne.

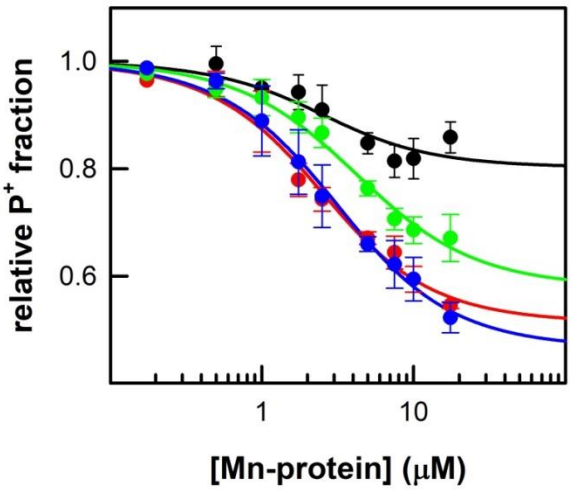

Figure 3.2. Titrations of P0, P1, P2 and P3 Mn-proteins to HHHH reaction centers. The relative P^+ fraction was determined using Equation 2.2 from Chapter 2, and the values were plotted against the different concentrations of Mn-protein. The data were fit to Equation 2.3 from Chapter 2, and the parameter we focused on was the dissociation constant, K_D. The dissociation constant value was 1.6, 1.7, 3.4 and 2.4 μM for the P0 (black circles), P1 (red circles), P2 (green circles) and P3 (blue circles) Mn-protein, respectively. The points above are taken from an average of three measurements and the error bars are standard deviation of the three measurements. The K_D values were determined from an average of three separate titrations.

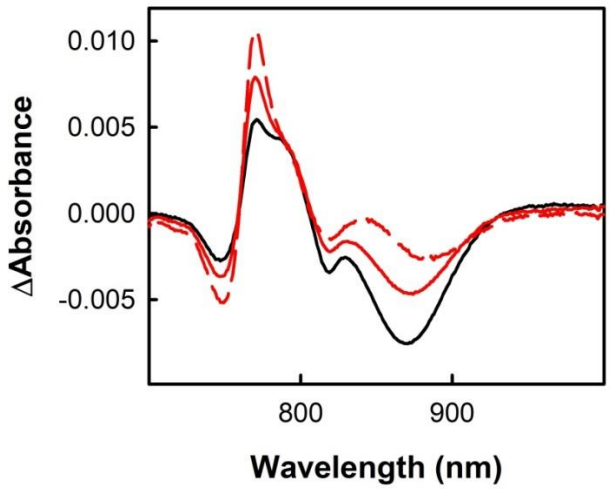

Figure 3.3. Representative light-minus-dark optical changes of HHHH reaction centers with and without the P1 Fe-protein show a range of activity. The HHHH reaction centers and terbutryne without the P1 Fe-protein show the characteristic decrease in extent of bleaching at 865 nm and the positive increase at 770 nm correlated with $P^{+}Q_{A}^{-}$ formation (black trace). Addition of 50 μM P1 Fe-protein to HHHH reaction centers and terbutryne (red traces) show the typical decrease in extent of bleaching at 865 nm and an increase in absorption at 770 nm, which is correlated to electron transfer from the P1 Fe-protein to HHHH reaction centers. The light-minus-dark spectra of HHHH reaction centers and terbutryne with the P1 Fe-protein varied in activity. The solid red trace shows low activity and the dashed red trace shows higher activity. The variation in activity prevented the characterization of the reaction. The assay conditions were the following: 1.5 μM HHHH reaction centers in 15 mM CHES (pH 9.4), 0.03 % Triton X-100 and 100 μM terbutryne.

Tables

Table 3.1. HHHH reaction center relative P^+ decrease with P1 Fe-protein.

dates	relative P^+ decrease
2015-09-12	0.08
2015-09-14	0.25
2015-09-19	0.11
2015-10-14	0.13
2015-12-18	0.10
2016-01-02	0.52
2016-01-09	0.32
2016-02-05	0.77
2016-03-11	0.54
2016-04-07	0.59
2016-04-08	0.60
Average values	0.36 ± 0.25

CHAPTER 4

BOUND MANGANESE OXIDES CAPABLE OF REDUCING THE BACTERIOCHLOROPHYLL DIMER OF MODIFIED BACTERIAL REACTION CENTERS FROM RHODOBACTER SPHAEROIDES

My contributions to the project were (i) purification of Mn12, Mn28, MD1-6, and MD1-7 reaction centers (ii) preparation of the manganese oxides (iii) the optical measurements with the manganese oxides and reaction centers, and (iv) I made figures to show the data I collected.

Abstract

The ability of Mn-oxides to bind to modified bacterial reaction centers and transfer an electron to the light-induced oxidized bacteriochlorophyll dimer, P^+, was characterized using optical spectroscopy. Two types of modifications of the reaction center are made to allow electron transfer from bound Mn-oxides. First, the environment of P is altered to obtain a high P/P^+ oxidation/reduction midpoint potential. Second, a variety of metal-binding sites are introduced by modification of amino acid residues as well as extension of the C-terminus of the M subunit. Each of the modified reaction centers is tested for binding and electron transfer to P^+ for a range of Mn-oxides, including αMn_2O_3, $CaMn_2O_4$, Mn_3O_4, and MnO_2, and compared to $MnCl_2$ and $Mn_3(PO_4)_2$. Steady-state optical spectra show P^+ reduction for each of the Mn-oxides, although to a lesser extent overall than for $MnCl_2$ and $Mn_3(PO_4)_2$, and the activity is generally inversely correlated with the initial oxidation state of the Mn-compound. Kinetic optical measurements with $CaMn_2O_4$ and αMn_2O_3 show a fast component, assigned to reduction by the Mn-oxide, in addition to a component due to charge recombination. In general, reaction centers with two of the binding sites showed significantly higher activity with the Mn-oxides, but those specific changes are not required, as reaction centers with the other binding sites also show activity.

Introduction

Multinuclear Mn-clusters facilitate critical oxidation/reduction reactions in enzymes such as Mn-catalase and photosystem II, with the transfer of electrons coupled to proton transfer.[18,29] To understand the properties of Mn-clusters in proteins, we are manipulating

the bacterial reaction center to bind Mn-oxides and characterizing the ability of the bound Mn-oxides to perform oxidation/reduction reactions. Our work makes use of previous studies where we have modified the reaction center to have the capability to oxidize Mn(II).[44]

The reaction center from *Rhodobacter sphaeroides* is a membrane-bound pigment-protein complex that performs the primary photochemistry in bacterial photosynthesis.[39] In the reaction center, light absorption by a bacteriochlorophyll dimer, P, initiates the transfer of an electron through intermediate electron acceptors to the primary quinone, Q_A, and then the secondary quinone, Q_B. To achieve the chemical capability to drive Mn-oxidation, we alter the reaction center to create a highly oxidizing dimer. The replacement of Leu M160, Leu L131 or Phe M197 to His results in the addition of hydrogen bonds to the conjugated system of P.[14] When the three modifications are made simultaneously, the P/P^+ midpoint potential is increased to 765 mV at pH 8.0 compared to the midpoint potential of 505 mV for wild-type reaction centers. Reaction centers with the high midpoint potential are shown to be able to oxidize Mn(II) in solution as well as dinuclear Mn-clusters bound to artificial proteins.[16, 25, 74, 75] Since this is a second-order reaction in both cases, only a single electron transfer could occur.

In order to create a first-order reaction potentially capable of producing high oxidations states by a bound Mn-cofactor, the highly oxidizing reaction centers are modified to bind Mn by the addition of possible Mn ligands at a location corresponding to that of the Mn_4CaO_5 of photosystem II, which is homologous to the reaction centers.[24] The reaction center mutant designated Mn12 contains the highly oxidizing P and

substitutions of Arg M164 to Tyr, Met M168 to Glu, and Gly M288 to Asp, and are found to bind mononuclear Mn(II) tightly. The positioning of Tyr at M164 creates a Tyr/His pair near the Mn-binding site analogous to the Y_Z (D1-161)/His D1-190 pair that participates in electron and proton transfer reactions of the Mn_4CaO_5 cluster. Optical spectroscopic measurements show that after light excitation and electron transfer, the bound Mn-cofactor is capable of rapidly and efficiently reducing P^+. Subsequently, highly oxidizing reaction centers containing the substitutions of Met M168 to Glu, Glu M173 to His, Val M192 to Glu, and Gly M288 to Asp, are also found to bind Mn(II) and are capable of light-driven oxygen production from superoxide.[76]

While the modified reaction centers provide several ligands for metal binding, opportunities to design additional ligands are limited without larger-scale changes to the protein. To introduce a more extensive binding site, we made use of the strong structural homology between bacterial reaction centers and photosystem II, which binds the Mn_4CaO_5 cluster, the site for water oxidation.[77-79] Alignment of the three-dimensional structures of the M subunit of reaction centers and the D1 subunit of photosystem II reveals a strong similarity in the five transmembrane regions, with the primary difference being the loop-helix-loop motif in the longer C-terminal region of the D1 subunit (Figure 4.1). The C-terminal extension provides many of the ligands that coordinate the Mn_4CaO_5 cluster and hence are not present in the bacterial reaction center. To add these possible ligands to the reaction center, the M subunit is modified with an extension of containing the C-terminal region of the D1 subunit. In addition, one of the key ligands identified in the assembly of the Mn_4CaO_5 cluster is Asp D1-170.[5,80] To investigate the possible

contribution of the equivalent residue, Glu M173, to Mn binding, reaction centers containing the C-terminal extension are constructed with either Glu or Asp at M173. Eight types of modified reaction centers with different combinations of characteristics are compared, along with two control strains (Figure 4.2).

The ability of the modified reaction centers to bind multinuclear Mn-compounds was investigated by the addition of Mn-oxides. We tested a suite of Mn-oxides, including Mn_3O_4, MnO_2, αMn_2O_3, and $CaMn_2O_4$, as well as $Mn_3(PO_4)_2$, whose synthesis has already been reported and which possess a range of oxidation states.[81-85] For example, the Mn in αMn_2O_3 can be poised in a (III, III) oxidation state. The Mn-compounds Mn_2O_3, MnO, MnO_2, Mn_3O_4, and $Mn_3(PO_4)_2$ have been electrochemically characterized as water oxidation catalysts.[82] The characterization of the Mn-oxides showed current densities below 0.100 mA/cm^2 at an overpotential value of 680 mV in comparison to 0.316 mA/cm^2 for $Mn_3(PO_4)_2$. The water oxidation catalytic activity of the Mn-oxides ranged in the following order from higher to lower: Mn_2O_3, MnO, MnO_2, and Mn_3O_4. Since the Mn-oxides are poorly soluble in aqueous solutions, procedures were developed that allowed the addition of suspensions of Mn-oxides at the μM concentrations required for the measurements. Steady-state light-minus-dark optical measurements were performed to indicate the extent to which the Mn-oxides could bind and reduce P^+ in different modified reaction centers. Transient optical measurements determined changes to the charge recombination rates and ability to transfer multiple electrons due to the presence of the bound Mn-oxides.

Materials and Methods

Design of reaction center modifications. Based upon the structural homology between the reaction centers and photosystem II, we designed a set of reaction centers that contain an extension to the M subunit consisting of the 30 C-terminal residues of the mature D1 subunit of photosystem II (Table B1). The five transmembrane helices are structurally well conserved between the two proteins. After helix E of the M subunit, which ends at Leu M286, there is a short loop followed by a small helix from Trp M294 to Gly M302. In photosystem II, the end of the E helix of the D1 subunit at Phe D1-295 is followed by an extended loop, an alpha helix from Trp D1-317 to Met D1-331, and then a loop from His D1-332 to the C-terminal residue Ala D1-344. This region contains five of the residues coordinating the Mn_4CaO_5 cluster, His D1-332, Glu D1-333, His D1-337, Asp D1-342, and Ala D1-344.

In order to incorporate these ligands for the Mn_4CaO_5 cluster into the reaction center, we designed extensions of the M subunit that includes the sequence from Asn D1-315 to Ala D1-344. This extension encodes the helix and terminal loop of D1 that follows the E transmembrane helix of D1. Based upon computer modeling of the structures, we placed as a bridge after the end of the M-subunit a GGNGGN linker. This type of linker has been used for other fusion constructions.[86] Thus the C-terminal residue of the M subunit connects to the linker and then to the D1 sequence. These modifications were added to changes that make P highly oxidizing, Leu L131, Leu M160, and Phe M197 to His, as well as Arg M164 to Tyr, producing the MD1-3 and MD1-4 reaction centers, that contain Glu and Asp at M173, respectively. To facilitate purification and ensure that the C-terminal sequence was present, the MD1-6 and MD1-7 reaction centers have the changes

of the MD1-3 and MD1-4 reaction centers with the addition of a 7-His tag at the end of the extended M subunit. For identification of role of the extended C-terminus, the Mn31 and Mn41 reaction centers contain the changes of the MD1-3 and MD1-4 reaction centers without the extension of the M subunit. A summary of the changes for the mutants is provided in Tables B1 and B2.

Mutagenesis. The wild type, T1, Mn12, and Mn28 reaction centers have been described previously.[14,24,76] The C-terminal extension of the M subunit containing the sequence from the D1 subunit was synthesized as an NcoI-BamHI fragment and substituted into an M subunit gene containing the additional mutations (Figure B1). Subsequent changes to the C-terminal region and the Glu (GAG) to Asp (GAT) change at M173 were made by oligo-directed mutagenesis.

Isolation of reaction centers from *Rhodobacter sphaeroides*. Reaction centers without a His-tag were isolated using previously described methods.[24] The reaction centers were dialyzed in 15 mM Tris(hydroxymethyl)aminomethane (Tris-Cl) (pH 8.0) and 0.05 % Triton X-100 before storage at –80°C. For optical measurements the reaction centers were equilibrated in 15 mM *n*-cyclohexyl-2-aminoethanesulfonic acid (CHES) (pH 9.4) and 0.025 % Triton X-100 using a 30000 molecular weight cut off (MWCO) Amicon filter.

Reaction centers with the His-tag were isolated following previous protocols.[87,88] Briefly, the cells were suspended in 50 mM sodium phosphate pH 8.0 and 150 mM sodium chloride. After lysis using a French Press (Simo Aminco), the reaction centers were solubilized by the addition of lauryldimethylamine-*N*-oxide (LDAO) to a final

concentration of 0.75 % for 15 min. The cell lysate was clarified using a Beckman L7 ultracentrifuge with a Ti45 rotor at 45000 rpm, for 40 minutes, at 4°C. After addition of 5 mM imidazole, the supernatant was loaded to a Ni-NTA column equilibrated in 50 mM sodium phosphate pH 8.0, 150 mM sodium chloride, 0.1 % LDAO and 5 mM imidazole. After washing in the equilibration solution, the reaction centers were eluted with 50 mM sodium phosphate pH 8.0, 150 mM sodium chloride, 0.1 % LDAO and 100 mM imidazole. The reaction centers were dialyzed against 15 mM Tris-Cl pH 8.0, 0.05 % Triton X-100 and 1 mM EDTA followed by ion-exchange chromatography. Reaction centers were bound to a DEAE column equilibrated in 15 mM Tris-Cl pH 8.0, 0.05 % Triton X-100 and 1 mM EDTA, washed, and eluted using a sodium chloride gradient with concentrations ranging from 50-120 mM. After concentration, the reaction centers were exchanged in 15 mM Tris-Cl pH 8.0 and 0.05 % Triton X-100 and stored at –80°C.

Preparation of Mn-oxides. Two Mn-oxides, MnO_2 and Mn_3O_4, were purchased from commercial sources (Sigma-Aldrich). Synthesis of αMn_2O_3, $CaMn_2O_4$, and $Mn_3(PO_4)_2$ followed procedures previously described.[81,82]

Particles of the manganese(III) oxide, αMn_2O_3, were synthesized by oxidation of manganese(II) ions in basic aqueous solution as previously described.[81] A 1 M ammonia solution with a volume of 50 mL was slowly added to 200 mL of a 30 mM $MnSO_4 \cdot H_2O$ solution, resulting in a formation of a brown precipitate. The mixture was stirred approximately 20 hours, at room temperature and exposed to air. A Sorvall centrifuge SA-600 rotor with centrifugal conditions of 13000 rpm, 20 minutes, at 4°C was used to collect the precipitate. Ultra-pure water was used to suspend and wash the precipitate,

which was collected by centrifugation as above. The precipitate was suspended in ultra-pure water and incubated in a drying oven (VWR 1305U) at 200°C for 48 hours.

Calcium-manganese(III) oxide particles, $CaMn_2O_4$, were synthesized similarly to αMn_2O_3 but with additional calcium ions present.[81] A 5-mL solution containing 470 mg $Ca(NO_3)_2 \cdot 4H_2O$ and 275 mg of $MnCl_2 \cdot 4H_2O$ in ultra-pure water was mixed with a 5-mL solution containing 95 mg of $KMnO_4$ and 8.4 g KOH in ultra-pure water. A precipitate formed and was collected using a CL-2 centrifuge (4°C, 3800 rpm, 60 minutes). After washing using water, the samples were centrifuged again. The precipitate was suspended in 10 mL of ultra-pure water and incubated at 200°C overnight in a drying oven (VWR 1305U).

Manganese(II) phosphate hydrate, $Mn_3(PO_4)_2$, was precipitated from aqueous solution following previously described protocols.[82] A 40-mL volume of 1 mM $MnCl_2$ in ultra-pure water and 40 mL of 1 mM KH_2PO_4 in 1.85 mM HEPES (pH 7.4) were mixed and incubated at 37°C for 20 hours. The $Mn_3(PO_4)_2$ particles were collected using a CL-2 centrifuge at 4000 rpm, for 15 minutes, at 4°C. A typical preparation yielded approximately 2 mg of wet flakes.

After synthesis, each of the Mn-oxides were washed to remove any free Mn(II). The powder was suspended in 1-mL of ultra-pure water and sonicated for 10 minutes. After dilution to a final volume of 50-mL in ultra-pure water, the Mn-oxides were pelleted using a CL-2 centrifuge (3800 rpm, 4°C, 30 min) for a total of three times. The final samples were dried at 200°C in a drying oven (VWR 1305U). The resulting compounds

were stored under vacuum. X-band EPR measurements confirmed the lack of any unreacted Mn(II) remaining from the synthesis in the Mn-oxide stocks (Figure B2).

Light-minus-dark optical measurements. Light-minus-dark optical measurements were made using a Varian Cary 6000i UV-Vis-near IR spectrometer (Agilent Technologies) with illumination by sub-saturating light from a 1000 W tungsten bulb with an 860 nm filter as previously described.[75] Reaction centers in 15 mM CHES (pH 9.4) and 0.025 % Triton X-100 were diluted to a final concentration of 1.5 μM reaction center in 15 mM CHES (pH 9.4), 0.025 % Triton X-100 and 100 μM terbutryne. Reaction centers were pre-illuminated for 2.5 min using light from 1000 W Tungsten bulb with an 860 nm filter. After a five-minute recovery from pre-illumination, the light-minus-dark optical spectrum was measured for reaction centers without Mn oxide. After the reaction centers were allowed to recover for another five minutes, the Mn-oxide was added.

For these measurements, the Mn-oxide stocks were treated as a suspension, since they do not dissolve in aqueous conditions. Prior to the measurements, hydrochloric acid was added to a concentration of 0.1 mM to create a better suspension without dissolution of the Mn oxide.[89] At this concentration of hydrochloric acid, no shift in pH value of the final solution was observed. The samples were sonicated for 10 minutes and stored at –80°C prior to measurement.

The Mn-oxide was added to achieve final concentrations of 2, 20 and 50 μM of the Mn-oxide. After each addition of Mn-oxide to the reaction center solution, a 5-minute wait in the dark allowed the binding of the Mn-oxide to the reaction centers, followed by

measurement of a light-minus-dark optical spectrum. For each concentration of Mn-oxide, measurement consisted of the steps of (i) a 5-minute recovery after illumination, (ii) addition of Mn-oxide to reaction centers, (iii) a 5-minute wait period after the addition, and (iv) measurement of the light-minus-dark optical spectrum.

The change in absorption of the P absorption band was used to determine the extent of P^+ reduction for each Mn-oxide by comparing the absorption change with and without the donor, (ΔA^{M}_{P-min}) and (ΔA^{0}_{P-min}), respectively:

$$\text{relative } P^+\text{fraction } = \frac{\Delta A^{M}_{P-min}}{\Delta A^{0}_{P-min}} \quad (4.1)$$

Since the peak wavelength position of P shifts slightly in the modified reaction centers, from 865 to 869 nm, measurements for each reaction center were performed at the wavelength where the absorption is zero in the light-minus-dark spectra when P^+ is fully reduced by the exogeneous donor diaminodurene.

Kinetic measurements of absorption changes at 865 nm. The kinetics measurements of the absorption changes at 865 nm were made using a Varian Cary 5. Reaction centers were at concentration of 1.5 µM in 15 mM CHES (pH 9.4), 0.025 % Triton X-100 and 100 µM terbutryne in a final volume of 1.0 mL. The reaction centers were pre-illuminated for 2.5 min using light from 1000 W Tungsten bulb with an 860 nm filter, and allowed to recover for 5 minutes. The reaction centers were illuminated using saturating 1-ns pulses at 532 nm from a Surelite SLI-10 Nd:YAG laser (Continuum). The absorbance at 865 nm was recorded for a 60 s time period with flashes at 10 sec, 25 sec and 40 sec of each trace. The reaction centers were given 5 minutes recovery time. The Mn-oxide was added a manner similar to the light-minus-dark optical changes. The Mn-

oxide concentration was 20 μM and 5 minutes were allowed for binding. The data were obtained by using a 60 sec measure time at 865 nm, and flashes were made at 10 sec, 25 sec and 40 sec.

Results

Steady-state optical spectroscopy showing redox activity of bound Mn-oxides. Light-minus-dark measurements are a sensitive means of identifying the presence of redox-active bound secondary donors to reaction centers. In wild-type reaction centers, illumination at 865 nm results in formation of the excited state of P, followed by electron transfer through a series of acceptors to the primary quinone acceptor, Q_A, and then the secondary quinone Q_B. The light-minus-dark spectrum shows a loss of absorption at 865 nm, corresponding to the presence of P^+, and electrochromic shifts near 760 and 800 nm, corresponding to the presence of $P^+Q_A^-$, as terbutryne was added to block transfer to Q_B. The spectra of the mutant reaction centers were similar to wild type, although with a lower amount of P^+ formed as a result of the increase in midpoint potential, as has been noted previously for these measurements of Mn12 and other mutants.[24,44]

Light-minus-dark spectra from 700 to 1000 nm were measured in the absence of the Mn-compounds, then in the presence of 2, 20, and 50 μM (see Table 4.1 for data at 20 μM). Activity of the Mn-compounds with the reaction centers was defined as a decrease in the absorption change at 865 nm as the amount of Mn-oxide was increased, consistent with a decrease in amount of P^+, with corresponding changes associated with Q_A^-. For the wild type reaction centers, the addition of the Mn-oxides resulted in no measureable change in the spectrum, consistent with a lack of electron transfer and showing that the

addition of the Mn-oxides does not cause degradation of the reaction center pigments. The T1 mutant, which has high P/P^+ midpoint potential but no metal binding site, showed no significant changes for addition at 20 μM of $CaMn_2O_4$, Mn_3O_4, and MnO_2, small changes of ~10% for αMn_2O_3 and larger decreases of ~20-30% for $MnCl_2$ and $Mn_3(PO_4)_2$. The activity with $MnCl_2$ results from second-order electron transfer as has been discussed previously.

Some activity was observed for each of the Mn-compounds in many of the reaction centers with a high midpoint potential and a metal binding site. Decreases of the absorption changes at 865 nm were correlated with the amount of Mn-oxide. For example, the MD1-6 reaction centers showed a decrease in the bleaching at 865 nm of ~20% and ~50% upon addition of 2 μM and 20 μM $CaMn_2O_4$, respectively (Figure 4.3). The addition of 50 μM of the Mn-compound decreased the P^+ fraction by an additional ~10 – 20% relative to the value at 20 μM, unless the P^+ fraction at 20 μM was already below 20% without the Mn-compound (Table B3). The extent of absorption changes for each Mn-compound was dependent upon the particular reaction center, and a full range of activities was observed, from 0 to 100% (Table 4.1). For example, the addition of 20 μM $CaMn_2O_4$ to Mn12, MD1-6, and Mn31 yielded absorption changes corresponding to P^+ fractions of 0.29, 0.51, and 0.69, respectively, compared to the spectra in the absence of added $CaMn_2O_4$ (Figure 4.4). In contrast, the addition of 20 μM MnO_2 to Mn12, MD1-6, and Mn31 yielded absorption changes corresponding to P^+ fractions of 0.91, 0.65, and 0.83, respectively compared to in the absence of added MnO_2 (Figure 4.5).

Kinetics measurements of electron transfer from Mn-oxides to P^+. The rate of $P^+Q_A^-$ charge recombination was measured by monitoring the absorption at 865 nm after a laser flash in the absence of Mn-oxide. The recoveries of the absorption had mono-exponential lifetimes of 32 ± 3, 44 ± 4, and 64 ± 6 ms for the T1, Mn12, and MD1-6 reaction centers respectively (Figure 4.6). The lifetimes for the T1 and Mn12 reaction centers are similar to previous measurements.[14,24] In the presence of 20 μM $CaMn_2O_4$, the recovery of the T1 reaction centers did not change, remaining mono-exponential with a time constant, 28 ± 3 ms, not significantly different that in the absence of $CaMn_2O_4$. In contrast, adequate fitting of the recoveries with the addition of $CaMn_2O_4$ required an additional component for the Mn12 and MD1-6 reaction centers. The lifetime of the faster component was 15 and 20 ms, for Mn12 and MD1-6 reaction centers, respectively, although a reliable determination of the values was prevented by their being comparable to the time resolution of 16 ms for the instrument. Similarly, in the presence of αMn_2O_3 the recovery of T1 reaction centers was unchanged, exhibiting a monoexponential rate corresponding to a time of 33 ± 2 ms, while the fits yielded an additional component with time constants of 15 and 25 ms for Mn12 and MD1-6 reaction centers, respectively.

The change in the amplitudes of the kinetic component attributed to $P^+Q_A^-$ charge recombination with the addition $CaMn_2O_4$ and αMn_2O_3 can be compared to the change in the P^+ fraction in the steady-state light-dark spectra. The amplitudes of the charge recombination components with the addition of $CaMn_2O_4$ were 25% and 40% of those of samples without the Mn-oxide for Mn12 and MD1-6, respectively. The decrease is consistent with the values of 29% and 51% determined for the P^+ fraction remaining in

the presence of $CaMn_2O_4$ measured by the light-minus-dark steady-state measurements (Table 4.1). Similar results were observed for samples with the addition of 20 μM αMn_2O_3, where the amplitudes were 20 and 35% compared to the sample without the Mn-oxide, in agreement with the 22 and 25% values for the P^+ fraction from the steady-state measurements (Table 4.1).

Discussion

In order to better understand the electronic properties of Mn-clusters in proteins, we characterized the capability of four different Mn-oxides, αMn_2O_3, $CaMn_2O_4$, Mn_3O_4, and MnO_2, to bind to modified reaction centers and transfer an electron to reduce P^+. In addition, the reaction centers were tested with the Mn-phosphate compound $Mn_3(PO_4)_2$ and $MnCl_2$, which had been previously characterized.[24, 76] To test measure the activity, we performed a steady-state optical assay using each of the Mn-compounds with reaction centers modified to have eight different metal binding sites, as well as two controls with no metal binding sites, wild type and T1, that has a highly oxidizing P. The results of this optical assay showed clear trends concerning the redox activity of the different Mn-oxides and the effectiveness of binding of the Mn-oxides to the different sites, as discussed below. We then discuss how this system provides the opportunity to investigate high oxidation states of Mn-clusters in proteins and the evolutionary implications.

Evidence for binding and electron transfer from Mn-oxides to reaction centers. The measured decreases in the amount of P^+ in the steady-state measurements are consistent with the reduction of P^+ by electron transfer from the Mn-compounds. The different measured values of the P^+ fraction shows that the extent of electron transfer is

dependent upon the specific combinations of Mn-oxides and modified reaction centers (Table 4.1). Consistent with the interpretation of electron transfer from the Mn-compounds is the addition of a fast kinetic component when a Mn-oxide was added, with the matching changes observed in the amplitudes when comparing the kinetic components and the P^+ fractions measured in the steady-state assay. The P^+ fraction values for most of the Mn-compounds are near 1.0 in the control reaction centers, the wild type and T1 reaction centers, showing that both a high P/P^+ midpoint potential and a binding site are required for high activity. Some activity was observed when $MnCl_2$ or $Mn_3(PO_4)_2$ was added to the highly oxidizing reaction centers, representing a second-order reaction as previously discussed.[16] Although the dissociation constants for the Mn-oxides were not determined because of the incomplete solubility of the compounds, the relatively small increase in activity from 20 to 50 μM indicates that by 20 μM, the majority of the binding of the Mn-oxides is complete.

Dependence of Mn-oxide activity on the binding site of the reaction center. The activities for reaction centers modified to have eight different metal binding sites were compared. These included four reaction centers, Mn12, Mn28, Mn31, and Mn41, with amino acid changes only in the body of the reaction center, and four reaction centers, MD1-3, MD1-4, MD1-6, and MD1-7, with a C-terminal extension of the M subunit that corresponds to the C-terminus region of the D1 subunit of photosystem II. For these modified reaction centers, the P^+ fraction representative of the activity with the Mn-oxides range from values of 0.08 to 0.96. In general, the Mn12 and Mn28 reaction

centers, which have been described previously[24,76], show the highest activity, with values as low as 0.1 for some of the Mn-oxides.

In designing the binding sites, we addressed the possibility of a role for M173, which is located at the analogous position to Asp D1-170, a key amino acid residue in the binding and photoassembly of the Mn_4CaO_5 cluster of photosystem II.[5] Wild-type reaction centers and the Mn31, MD1-3, and MD1-6 reaction centers contain Glu M173. The substitution of M173 to Asp was made in three of the reaction centers, Mn41, MD1-4, and MD1-6, which are otherwise identical to Mn31, MD1-3, and MD1-7 reaction centers, respectively. For some combinations, the reaction centers that were identical except for the presence of Glu or Asp at M173 have similar activities, for example values of 0.72 and 0.73 were obtained for $CaMn_2O_4$ with the MD1-3 and MD1-4 reaction centers, respectively. However, as a trend the reaction centers with Glu at M173 had up to a ~10% higher activity than those with Asp at M173 (Figure 4.7). These results indicate that M173 is not a crucial residue for binding of the Mn-compounds. The exception is the MD1-6 reaction centers with $Mn_3(PO_4)_2$, αMn_2O_3, and $CaMn_2O_4$, where the activity was ~40% higher than in MD1-7, indicating that the Glu M173 acts synergistically with the C-terminal extension to bind an active Mn-compound.

Dependence of Mn-oxide activity on the oxidation state of the Mn-compound. Overall, $MnCl_2$ and $Mn_3(PO_4)_2$ showed the greatest activity, while Mn_3O_4 and MnO_2 showed the least activity (Figure 4.8). A general trend is evident with the activity being correlated with the oxidation states of the Mn. For example, $MnCl_2$ and $Mn_3(PO_4)_2$ have Mn in the (II) and (II,II,II) oxidation states and show the highest activities with average

values of 0.14 and 0.24, respectively. The lowest activities are associated with Mn-oxides with higher oxidation states of Mn. For example, MnO_2 has Mn in the (IV) oxidation state and shows the least activity with an average value of 0.85. The other three compounds, αMn_2O_3, $CaMn_2O_4$, Mn_3O_4, have Mn in the intermediate (III,III) or (II,III,III) oxidation states and average P+ fractions of 0.38, 0.63, and 0.82, respectively. It is likely that this trend reflects higher midpoint potentials for the III to IV and IV to V transitions of the oxidation states of the Mn compared to the II to III transition rather than differences in the binding of the Mn-oxides. Despite an apparent high midpoint potential for MnO_2, significant activity is observed when bound to the MD1-6 reaction centers, demonstrating the capability of the highly oxidizing reaction centers to convert light energy into high oxidation states of Mn-cofactors.

Mn-oxides as precursor donors in the primitive oxygen-evolving complex. The Mn_4CaO_5 cluster of photosystem II undergoes a self-assembly process, termed photoactivation or photoassembly, utilizing the conversion of light energy to drive the oxidation of bound Mn(II) into a catalytically active cluster.[5,80,90-92] Despite its critical role in photosynthesis, the specific mechanism of how the Mn_4CaO_5 cluster of photosystem II is formed is poorly understood, in particular the nature of intermediate states of the Mn-cofactor.

Our strategy of using Mn-oxides is inspired by their capacity to serve as water oxidation catalysts and the conjecture that primitive water-oxidizing complexes incorporated natural marine Mn-oxides.[92-96] Analysis of protein sequences has identified evolutionary developments from anoxygenic to oxygenic photosynthesis, but the process

that gave rise to the development of the Mn_4CaO_5 cluster remains unknown. The evolution presumably developed in the absence of the complete binding site for the Mn_4CaO_5 cluster and mechanism for self-assembly. The requirement for these developments could have been bypassed by primitive phototrophs by the binding of Mn-oxides present in low concentrations in the aqueous environment. Mn-oxides have the capability of water oxidation in the presence of a strong chemical oxidant, enabling the establishment of water oxidation in the ancient protein complexes.[92] The ability of the Mn-oxides to bind to the reaction center and transfer electrons is supportive of the feasibility of this conjecture.

We have examined the ability of different Mn-oxides to bind and serve as electron transfer donors to P^+. Our results strongly suggest that protein complexes can bind active Mn-oxides that can function as bound secondary donors to reduce the oxidized primary electron donor. Mn-oxides mixed with apo-photosystem II have been examined in the bulk by measurements such as voltammetry without determination of the binding or investigation of the individual electron transfer processes.[97] While we are not duplicating the mechanisms involving the Mn_4CaO_5 cluster of photosystem II, these results demonstrate that bacterial reaction center can serve as a model system for probing the electron transfer reactions involving bound of Mn-oxides serving as secondary electron donors, producing high oxidation states.

Acknowledgments

We thank Dimah Abdullah for her assistance with some of the laboratory work.

Figures

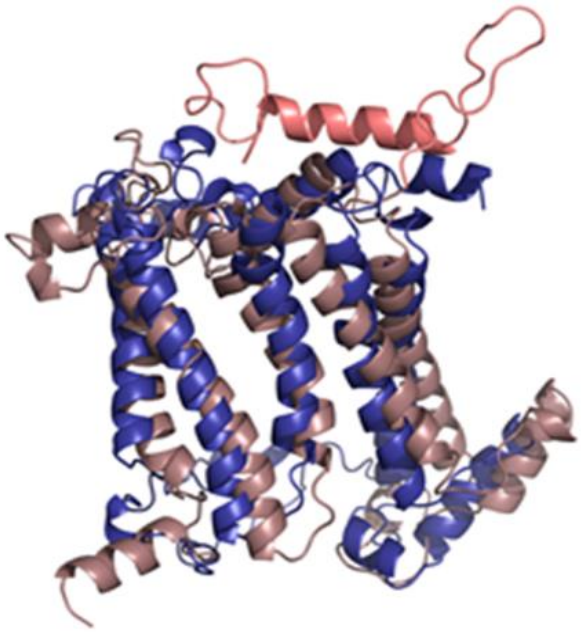

Figure 4.1. Comparison of M subunit and D1 subunit structures. Overlay of the M subunit of reaction centers (blue) and the D1 subunit of photosystem II (dark red) highlights the structural similarity of the five trans-membrane helices. The key difference is that the D1 subunit has a loop-helix-loop at the C-terminus that the M subunit does not have, and the loop-helix-loop is important in binding the oxygen-evolving complex. Our MD1 reaction centers incorporate the loop-helix-loop of the D1 subunit at the C-terminus of the M subunit via a glycine linker.

	H-bond			binding site					C-term
WT*	L	L	F	M	G	V	E		
T1	H	H	H	M	G	V	E		
Mn12	H	H	H	E	D	V	E		
Mn28	H	H	H	E	D	E	H		
Mn31	H	H	H	M	G	E	E		
MD1-3	H	H	H	M	G	E	E	D1	
MD1-6	H	H	H	M	G	E	E	D1	H-tag
Mn41	H	H	H	M	G	E	D		
MD1-4	H	H	H	M	G	E	D	D1	
MD1-7	H	H	H	M	G	E	D	D1	H-tag

Figure 4.2. Comparison of the design characteristics of modified reaction centers. Each of the modified reaction centers has differences from the WT* reaction center, which contains the wild-type amino acid sequence. All of the modified reaction centers contain the changes, Leu L131 to His, Leu M160 to His, and Phe M197 to His (highlighted in pink), that result in hydrogen bonds to P and an increase of 260 mV in the P/P^+ midpoint potential relative to wild type. The metal-binding sites modifications (highlighted in green) differ in the residues Met M168, Gly M288, Val M192, and Glu M173, with three of the modified reaction centers having Asp M173 (highlighted in cyan) at the position corresponding to Asp 170 of the D1 subunit of photosystem II. Additional amino acid residues from the C-terminus of the D1 subunit of photosystem II connected to the C-terminus of the M subunit by a GGNGG linker (Table B2) were planned for the MD1-3, MD1-4, MD1-6, and MD1-7 reaction centers (highlighted in bright green), with a 7x-His tag (highlighted in yellow) added at the C-terminus of the M subunit in the MD1-6 and MD1-7 reaction centers.

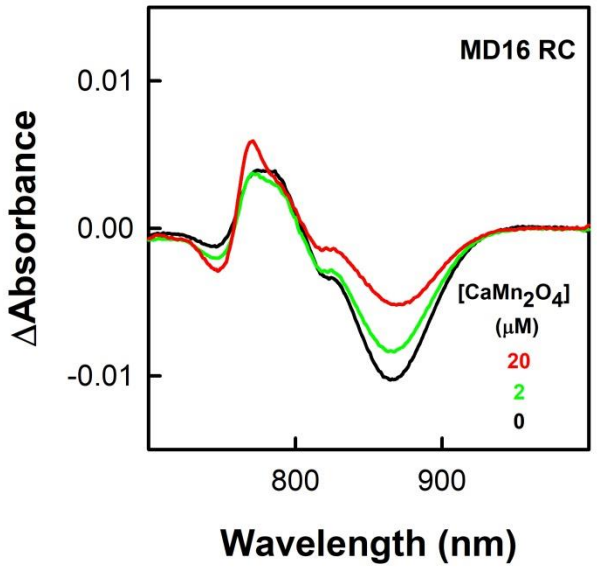

Figure 4.3. Optical changes in MD1-6 reaction centers at varying oxide concentrations. Light-minus-dark spectra of reaction centers and terbutryne without oxide (black trace) show a decrease in absorption at 865 nm and a positive increase at 770 nm consistent with a formation of $P^+Q_A^-$. The MD1-6 reaction centers and terbutryne with 2 μM $CaMn_2O_4$ (green) and 20 μM $CaMn_2O_4$ (red) show a decrease in extent of bleaching at 865 nm compared to reaction centers and terbutryne without $CaMn_2O_4$. The P^+ fraction decreased to the values of 0.82 and 0.50 for 2 and 20 μM $CaMn_2O_4$, respectively. The assay conditions were the following: 1.5 μM MD1-6 reaction centers in 15 mM CHES (pH 9.4), 0.025 % Triton X-100 and 100 μM terbutryne.

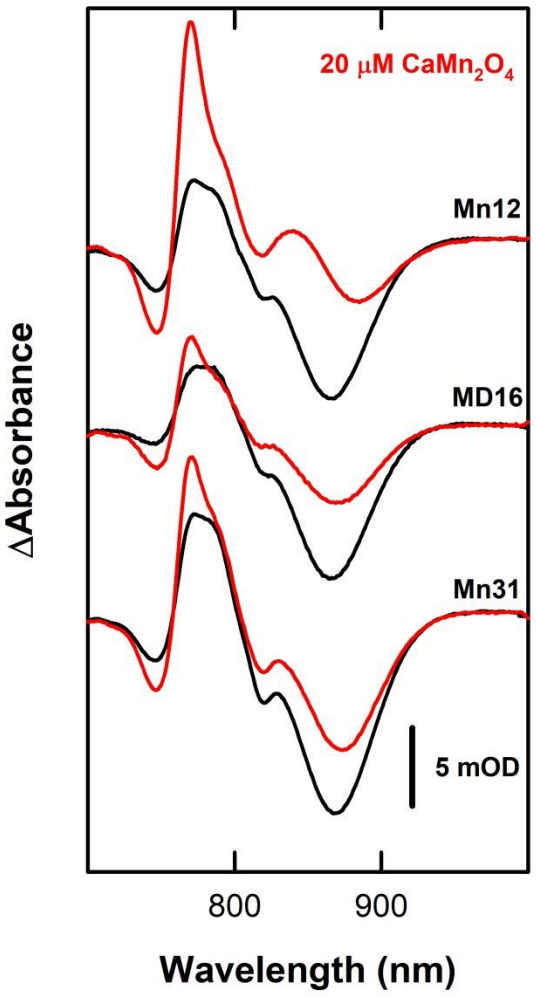

Figure 4.4. Optical changes of reaction centers with $CaMn_2O_4$. Shown are light-minus-dark spectra of Mn12 (top), MD1-6 (middle) and Mn31 (bottom) reaction centers with (red traces) and without (black traces) 20 μM $CaMn_2O_4$. The P^+ fraction decreased to 0.31, 0.50, and 0.67 for Mn12, MD1-6, and Mn31 reaction centers, respectively. The assay conditions were: 1.5 μM reaction center in 15 mM CHES (pH 9.4), 0.025 % Triton X-100 and 100 μM terbutryne.

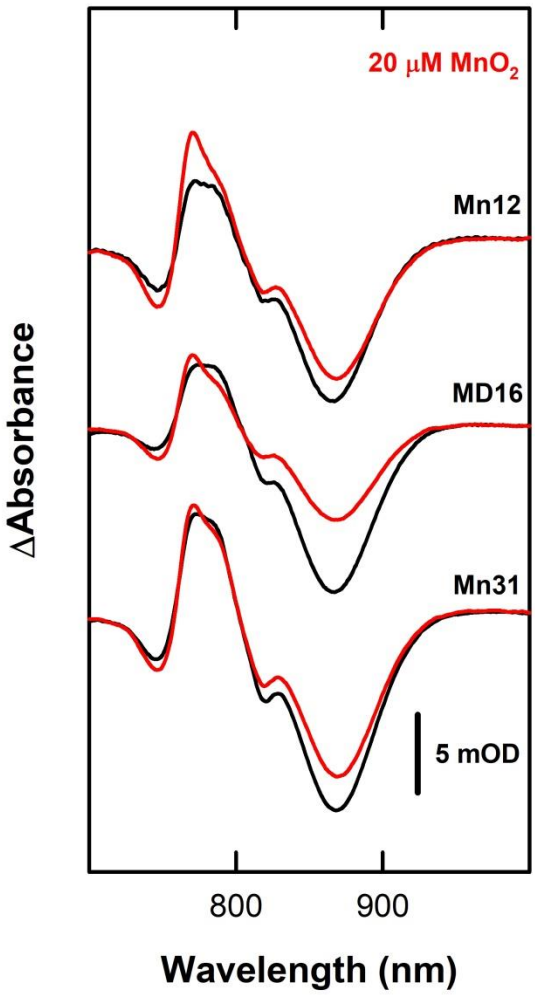

Figure 4.5. Optical changes of reaction centers with MnO_2. Shown are light-minus-dark spectra of Mn12 (top), MD1-6 (middle) and Mn31 (bottom) reaction centers with (red traces) and without (black traces) 20 μM MnO_2. The P^+ fraction decreased to 0.85, 0.56, and 0.83 for Mn12, MD1-6, and Mn31 reaction centers, respectively. The assay conditions were: 1.5 μM reaction center in 15 mM CHES (pH 9.4), 0.025 % Triton X-100 and 100 μM terbutryne.

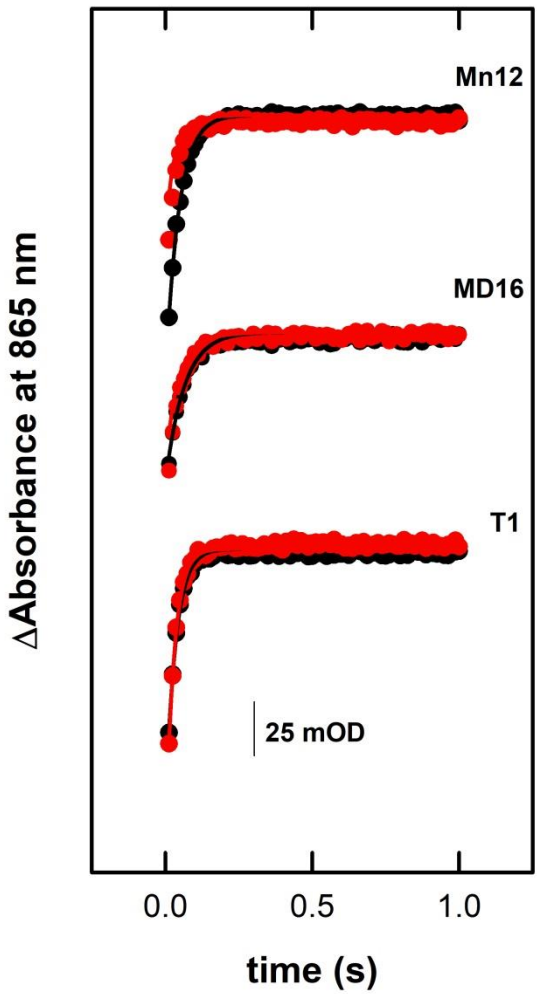

Figure 4.6. Decay of absorption changes at 865 nm in reaction centers with $CaMn_2O_4$. Shown are the decay traces of Mn12 (top), MD1-6 (middle), and T1 (bottom) reaction centers with (red traces) and without (black traces) 20 μM $CaMn_2O_4$. The Mn12, MD1-6, and T1 reaction centers without $CaMn_2O_4$ were fit to mono-exponential decay with lifetimes of 44 ± 4, 64 ± 6, and 32 ± 3 ms, respectively. For the T1 reaction centers with 20 μM $CaMn_2O_4$, the absorption changes were very similar, fitting with a monoexponential with a time constant of 28 ± 3 ms. For the Mn12 and MD1-6, reaction centers, fitting required an additional component, with time constants of 15 and 20 ms respectively. These components are attributed to electron transfer from the $CaMn_2O_4$ oxide. The assay conditions were: 1.5 μM reaction centers in 15 mM CHES (pH 9.4), 0.025 % Triton X-100 and 100 μM terbutryne.

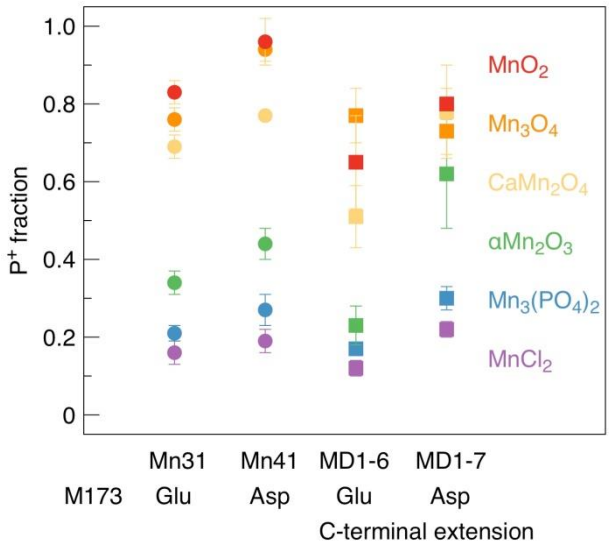

Figure 4.7. Comparison of the P^+ fraction for the different Mn-compounds at 20 μM concentrations for four of the modified reaction centers. Shown are the P^+ fractions for the Mn31, Mn41, MD1-6 and MD1-7 reaction centers in the presences of various Mn-compounds. The activity of the bound Mn-compound results in the loss of the P^+ fraction.

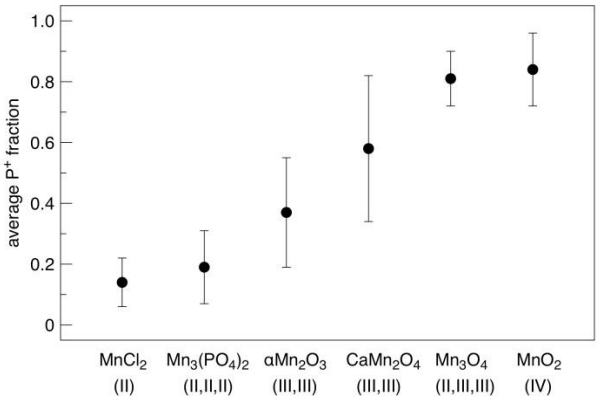

Figure 4.8. Comparison of the average of the extent of the P^+ fraction for the different Mn-compounds at 20 μM concentrations. Plotted is the average of the P^+ fraction at 20 μM of Mn compounds for the reaction centers with metal-binding sites (Mn12, Mn28, Mn31, Mn41, MD1-3, MD1-4, MD1-6, MD1-7).

Tables

Table 4.1. Relative P^+ fraction values at a 20 μM concentration of Mn-compounds.

Reaction center	P^+ fraction					
	MnO_2	$CaMn_2O_4$	αMn_2O_3	Mn_3O_4	$Mn_3(PO_4)_2$	$MnCl_2$
WT	1.01 ± 0.03	1.00 ± 0.01	1.01 ± 0.01	0.99 ± 0.01	1.03 ± 0.01	1.04 ± 0.01
T1	1.01 ± 0.05	1.04 ± 0.10	0.90 ± 0.04	0.97 ± 0.05	0.80 ± 0.05	0.68 ± 0.03
Mn12	0.91 ± 0.05	0.29 ± 0.08	0.22 ± 0.07	0.91 ± 0.04	0.02 ± 0.01	0.02 ± 0.01
Mn28	0.71 ± 0.03	0.14 ± 0.06	0.08 ± 0.04	0.72 ± 0.07	0.01 ± 0.01	0.01 ± 0.00
Mn31	0.83 ± 0.03	0.69 ± 0.03	0.34 ± 0.03	0.76 ± 0.02	0.21 ± 0.02	0.16 ± 0.03
Mn41	0.96 ± 0.06	0.77 ± 0.01	0.44 ± 0.05	0.94 ± 0.03	0.27 ± 0.03	0.19 ± 0.02
MD1-3	0.90 ± 0.04	0.72 ± 0.04	0.45 ± 0.04	0.79 ± 0.05	0.20 ± 0.02	0.15 ± 0.01
MD1-4	0.98 ± 0.02	0.73 ± 0.06	0.54 ± 0.06	0.89 ± 0.01	0.32 ± 0.04	0.23 ± 0.03
MD1-6	0.65 ± 0.12	0.51 ± 0.07	0.24 ± 0.05	0.77 ± 0.08	0.17 ± 0.02	0.12 ± 0.02
MD1-7	0.80 ± 0.03	0.78 ± 0.12	0.62 ± 0.14	0.73 ± 0.06	0.30 ± 0.03	0.22 ± 0.02

CHAPTER 5

CONCLUSIONS

Outlook

My thesis work addresses general questions concerning the Mn cluster of photosystem II (PSII) by characterizing manganese oxidation in modified bacterial reaction centers from *Rhodobacter sphaeroides*. I specifically focused on characterizing one-electron reduction-oxidation reactions from multi-nuclear Mn cofactors to modified bacterial reaction centers. I worked with an array of artificial di-nuclear proteins as was presented in Chapter 2 and Chapter 3. The highlight of my work with Mn-proteins is the light-induced electron transfer from artificial Mn-proteins to P^+ in reaction centers. I also worked with metal-binding bacterial reaction centers with modifications made to mimic the binding site of the manganese-calcium-oxide cluster in PSII. In Chapter 4, I presented the binding and oxidation of multi-nuclear Mn oxides in the metal-binding bacterial reaction centers. My thesis work is the transition to characterization of multiple turnovers due to light-induced oxidation of multi-nuclear metal cofactors in reaction centers.

One future direction of research is the characterization of light-driven enzymatic activity of biologically relevant reactions. The metal-binding reaction centers incorporate structural modifications that introduce carboxylate ligands to bind metal cofactors, which catalyze chemical reactions. For example, Mn-binding reaction centers are able to make use of superoxide as a substrate in reactions that resemble those of Mn-superoxide dismutase.[76] Similarly, enzymatic redox reactions have been catalyzed by di-iron active sites in artificial four-helix *due ferri* (DF) proteins.[98] My hypothesis is that light-driven

oxygen-activating enzymatic reactions would be enabled as a consequence of achieving reaction centers capable of binding and oxidizing ferrous ions.

A second project I would pursue is light-driven assembly of a multi-nuclear cofactor in the metal-binding reaction center. The initial step would be the binding of Mn followed by characterization of a second Mn capable of binding to reaction centers and reducing P^+. Currently, the first electron transfer from Mn to P^+ in metal-binding reaction centers has been extensively characterized in the presence of terbutryne, an inhibitor of electron transfer to the terminal quinone.[10] In the absence of terbutryne, electron transfer proceeds to the secondary quinone, forming Q_B^-, and a second electron transfer produces the doubly-reduced, doubly protonated secondary quinone. In order to achieve a second electron transfer with good yield, I propose to slow down the charge-recombination rate from Q_B^- to P^+, as has been done previously by modification of wild-type reaction centers.[99] One complication is that formation of the doubly-reduced terminal quinone is slower in these modified reaction centers, but one way to mitigate the effect is to allow longer intervals between laser pulses to allow forward electron transfer to the terminal quinone. My hypothesis is that as a consequence of slowing down the $P^+Q_B^-$ charge-recombination rate, the yield of formation of the Mn_X^+:PQ_B^- state would increase in the metal-binding reaction centers, which in turn would allow for light-driven formation of a PQ_B^{-2} state after binding and electron transfer from a second Mn ion (Figure 5.1).

Finally, my thesis addresses the hypothesis that the Mn_4CaO_5 cluster evolved from Mn minerals that were incorporated in a primitive photosynthetic protein.[93] My studies with reaction centers are not attempts to replicate the biochemical processes in PSII

rather my studies inform about the conditions prior to the advent of oxygenic photosynthesis. In Chapter 4, I provide evidence of electron transfer from bound Mn-oxides in structurally modified reaction centers. The results in Chapter 4 suggest that a primitive photosynthetic protein could have incorporated a Mn cluster from a Mn mineral. I speculate that a Mn mineral would need to come in contact with the primitive photosynthetic protein to allow for the incorporation of the Mn cluster into a binding pocket.

Figures

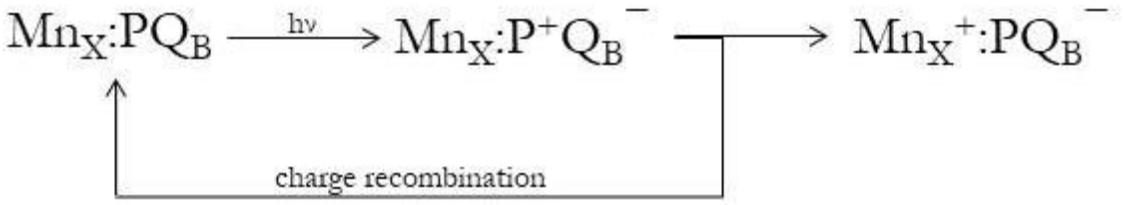

Figure 5.1. Electron transfer in reaction centers with a bound Mn cofactor. Upon absorption of a photon P is excited to P*, and formation of $P^+Q_B^-$ occurs. In the presence of bound Mn_X there are two possibilities for electron transfer. One possibility is the recombination from $P^+Q_B^-$ to PQ_B. A second possibility is electron transfer from Mn_X to P^+ yielding $Mn_X^+:PQ_B^-$. Mn_X oxidation in Mn12 reaction centers is well characterized, but the second turnover is not well understood. To maximize the oxidation of Mn_X in Mn12 reaction centers, the additional modification of Glu L212 to Gln L212 would slow down the charge recombination. A slower charge recombination should favor the oxidation of Mn_X cofactor to a greater extent.

REFERENCES

(1) Eisenberg, R. (2018) Addressing the challenge of carbon-free energy. *ACS Energy Lett. 3*, 1521–1522.

(2) Jin, S. (2018) What else can photoelectrochemical solar energy conversion do besides water splitting and CO_2 reduction? *ACS Energy Lett. 3*, 2610–2612.

(3) Berardi, S., Drouet, S., Francas, L., Gimber-Surinach, C., Guttentag, M., Richmond, C., Stoll, T., and Llobet, A. (2014) Molecular artificial photosynthesis. *Chem. Soc. Rev. 43*, 7501–7519.

(4) Barber, J. (2009) Photosynthetic energy conversion: natural and artificial. *Chem. Soc. Rev. 38*, 185–196.

(5) Bao, H. and Burnap, R. L. (2016) Photoactivation: The light-driven assembly of the water oxidation complex of photosystem II. *Front. Plant Sci. 7*, 57B.

(6) Kálmán, L., Williams, J. C., and Allen, J. P. (2008) Comparison of bacterial reaction centers and photosystem II. *Photosynth. Res. 98*, 643–655.

(7) Allen, J. P., and Williams, J. C. (1998) Photosynthetic reaction centers. *FEBS Lett. 438*, 5–9.

(8) Wang, H., Hao, Y., Jiang, Y., Lin, S., and Woodbury, N. W. (2012) Role of protein dynamics in guiding electron-transfer pathways in reaction centers from *Rhodobacter sphaeroides*. *J. Phys. Chem. B 116*, 711–717.

(9) Okamura, M. Y., Paddock, M. L., Graige, M. S., and Feher, G. (2000) Proton and electron transfer in bacterial reaction centers. *Biochim. Biophys. Acta 1458*, 148–163.

(10) Olson, T. L., Williams, J. C., and Allen, J. P. (2013) Influence of protein interactions on oxidation/reduction midpoint potentials of cofactors in natural and de novo metalloproteins. *Biochim. Biophys. Acta 1827*, 914–922.

(11) Allen, J. P., Feher, G., Yeates, T. O., Komiya, H., and Rees, D. C. (1987) Structure of the reaction center from *Rhodobacter sphaeroides* R-26: The protein subunits. *Proc. Natl. Acad. Sci. U. S. A. 84*, 6162–6166.

(12) Allen, J. P., Feher, G., Yeates, T. O., Komiya, H., and Rees, D. C. (1987) Structure of the reaction center from *Rhodobacter sphaeroides* R-26: The cofactors. *Proc. Natl. Acad. Sci. U. S. A/ 84*, 5730–5734.

(13) Yeates, T. O., Komiya, H., Rees, D. C., Allen, J. P., and Feher, G. (1987) Structure of the reaction center from *Rhodobacter sphaeroides* R-26: Membrane-protein interactions. *Proc. Natl. Acad. Sci. U. S. A. 84*, 6438–6442.

(14) Lin, X., Murchison, H. A., Nagarajan, V., Parson, W. W., Allen, J. P., and Williams, J. C. (1994) Specific alteration of the oxidation potential of the electron donor in reaction centers from *Rhodobacter sphaeroides*. *Proc. Natl. Acad. Sci. U. S. A. 91*, 10265–10269.

(15) Kálmán, L., LoBrutto, R., Allen, J. P., and Williams, J. C. (1999) Modified reaction centres oxidize tyrosine in reactions that mirror photosystem II. *Nature 402*, 696–699.

(16) Kálmán, L., LoBrutto, R., Allen, J. P., and Williams, J. C. (2003) Manganese oxidation by modified reaction centers from *Rhodobacter sphaeroides*. *Biochemistry 42*, 11016–11022.

(17) Najafpour, M. M., Ghobadi, M. Z., Haghighi, B., Tomo, T., Shen, J. R., and Allakhverdiev, S. L. (2015) Comparison of nano-sized Mn oxides with the Mn cluster of photosystem II as catalysts for water oxidation. *Biochim. Biophys. Acta 1847*, 294–306.

(18) Armstrong, F. A. (2008) Why did Nature choose manganese to make oxygen? *Phil. Trans. R. Soc. B 363*, 1263–1270.

(19) Johnson, K. S. (2006) Manganese redox chemistry revisited. *Science 313*, 1896–1897.

(20) McConnell, I., Li, G., and Brudvig, G. W. (2010) Energy conversion in natural and artificial photosynthesis. *Chem. Biol. 17*, 434–447.

(21) Najafpour, M. M., Erenberg, T., Wiechen, M., and Kurz, P. (2010) Calcium manganese(III) oxides ($CaMn_2O_4 \bullet xH_2O$) as biomimetic oxygen-evolving catalysts. *Angew. Chem. Int. Ed. 49*, 2233–2237.

(22) McConnell, I. L. (2008) Substrate water binding and oxidation in photosystem II. *Photosynth. Res. 98*, 261–276.

(23) Komiya, H., Yeates, T. O., Rees, D. C., Allen, J. P., and Feher, G. (1988) Structure of the reaction center from *Rhodobacter sphaeroides* R-26 and 2.4.1: Symmetry relations and sequence comparisons between different species. *Proc. Natl. Acad. Sci. U. S. A. 85*, 9012–9016.

(24) Thielges, M., Uyeda, G., Camara-Artigas, A., Kálmán, L., Williams, J. C., and Allen, J. P. (2005) Design of a redox-linked active metal site: Manganese bound to bacterial reaction centers at a site resembling that of photosystem II. *Biochemistry 44*, 7389–7394.

(25) Kálmán, L., Williams, J. C., and Allen, J. P. (2011) Energetics for oxidation of a bound manganese cofactor in modified bacterial reaction centers. *Biochemistry 50*, 3310–3320.

(26) Kálmán, L., LoBrutto, R., Williams, J. C., and Allen, J. P. (2006) Iron as a bound secondary electron donor in modified bacterial reaction centers. *Biochemistry 45*, 13869–13874.

(27) Calhoun, J. R., Nastri, F., Maglio, O., Pavone, V., Lombardi, A., and DeGrado, W. F. (2005) Artificial diiron proteins: From structure to function. *Biopolymers 80*, 264–278.

(28) Mandal, S., Espiritu, E., Akram, N., Lin, S., Williams, J. C., Allen, J. P., and Woodbury, N. W. (2018) Influence of the electrochemical properties of the bacteriochlorophyll dimer on triplet energy-transfer dynamics in bacterial reaction centers. *J. Phys. Chem. B 122*, 10097–10107.

(29) Sigel, A., and Sigel, H., Eds. (2000) *Manganese and its role in biological processes*, Marcel Dekker, NY.

(30) Farid, T. A., Kodali, G., Solomon, L. A., Lichtenstein, B. R., Sheehan, M. M., Fry, B. A., Bialas, C., Ennist, N. M., Siedlecki, J. A., Zhao, Z., Stetz, M. A., Valentine, K. G., Anderson, J. L. R., Wand, A. J., Discher, B. M., Moser, C. C., and Dutton, P. L. (2013) Elementary tetrahelical protein design for diverse oxidoreductase functions. *Nat. Chem. Biol. 9*, 826–833

(31) Yu, F., Cangelosi, V. M., Zastrow, M. L., Tegoni, M., Plegaria, J. S., Tebo, A. G., Mocny, C. S., Ruckthong, L., Qayyum, H., and Pecoraro, V. L. (2014) Protein design: Toward functional metalloenzymes. *Chem. Rev. 114*, 3495−3578.

(32) Chino, M., Maglio, O., Nastri, F., Pavone, V., DeGrado, W. F., and Lombardi, A. (2015) Artificial diiron enzymes with a de novo designed four-helix bundle structure. *Eur. J. Inorg. Chem. 2015*, 3371–3390.

(33) Regan, L., Caballero, D., Hinrichsen, M. R., Virrueta, A., Williams, D. M., and O'Hern, C. S. (2015) Protein design: Past, present, and future. *Biopolymers 104*, 334–350.

(34) Brisendine, J. M., and Koder, R. L. (2016) Fast, cheap and out of control — Insights into thermodynamic and informatic constraints on natural protein sequences from *de novo* protein design. *Biochim. Biophys. Acta 1857*, 485–492.

(35) Hosseinzadeh, P., and Lu, Y. (2016) Design and fine-tuning redox potentials of metalloproteins involved in electron transfer in bioenergetics. *Biochim. Biophys. Acta 1857*, 557–581.

(36) Peacock, A. F. A. (2016) Recent advances in designed coiled coils and helical bundles with inorganic prosthetic groups – from structural to functional applications. *Curr. Opin. Chem. Biol. 31*, 160–165.

(37) Di Costanzo, L., Wade, H., Geremia, S., Randaccio, L., Pavone, V., DeGrado, W. F., and Lombardi, A. (2001) Toward the de novo design of a catalytically active helix bundle: A substrate-accessible carboxylate-bridged dinuclear metal center. *J. Am. Chem. Soc. 123*, 12749–12757.

(38) Maglio, O., Nastri, F., Torres Martin de Rosales, R., Faiella, M., Pavone, V., DeGrado, W. F., and Lombardi, A. (2007) Diiron-containing metalloproteins: Developing functional models. *C. R. Chim. 10*, 703–720.

(39) Hunter, C. N., Daldal, F., Thurnauer, M. C., and Beatty, J. T., Eds. (2009) *The Purple Phototrophic Bacteria*, Springer-Verlag, Dordrecht, The Netherlands.

(40) Axelrod, H. L., Abresch, E. C., Okamura, M. Y., Yeh, A. P., Rees, D. C., and Feher, G. (2002) X-ray structure determination of the cytochrome c_2: reaction center electron transfer complex from *Rhodobacter sphaeroides*. *J. Mol. Biol. 319*, 501–515.

(41) Axelrod, H. L., and Okamura, M. Y. (2005) The structure and function of the cytochrome c_2: reaction center electron transfer complex from *Rhodobacter sphaeroides*. *Photosynth. Res. 85*, 101–114.

(42) Cramer, W. A., Hasan, S. S., and Yamashita, E. (2011) The Q cycle of cytochrome *bc* complexes: A structure perspective. *Biochim. Biophys. Acta 1807*, 788–802.

(43) Allen, J. P., and Williams, J. C. (2014) Energetics of cofactors in photosynthetic complexes: Relationship between protein-cofactor interactions and midpoint potentials, in *The Biophysics of Photosynthesis* (Goldbeck, J., and van der Est, A., Eds.), pp 275–299, Springer-Verlag, Dordrecht, The Netherlands.

(44) Müh, F., Lendzian, F., Roy, M., Williams, J. C., Allen, J. P., and Lubitz, W. (2002) Pigment-protein interactions in bacterial reaction centers and their influence on oxidation potential and spin density distribution of the primary donor. *J. Phys. Chem. B 106,* 3226–3236.

(45) Lin, X., Williams, J. C., Allen, J. P., and Mathis, P. (1994) Relationship between rate and free energy difference for electron transfer from cytochrome c_2 to the reaction center in *Rhodobacter sphaeroides*. *Biochemistry 33,* 13517–13523.

(46) Olson, T. L., Espiritu, E., Edwardraja, S., Simmons, C. R., Williams, J. C., Ghirlanda, G., and Allen, J. P. (2016) Design of dinuclear manganese cofactors for bacterial reaction centers. *Biochim. Biophys. Acta 1857,* 539–547.

(47) Olson, T. L., Espiritu, E., Edwardraja, S., Canarie, E., Flores, M., Williams, J. C., Ghirlanda, G., and Allen, J. P. (2017) Biochemical and spectroscopic characterization of dinuclear Mn-sites in artificial four-helix bundle proteins. *Biochim. Biophys. Acta 1858,* 945–954.

(48) Flores, M., Olson, T. L., Wang, D., Edwardraja, S., Shinde, S., Williams, J. C., Ghirlanda, G., and Allen, J. P. (2015) Copper environment in artificial metalloproteins probed by electron paramagnetic resonance spectroscopy. *J. Phys. Chem. B 119,* 13825–13833.

(49) Williams, J. C., and Allen, J. P. (2009) Directed modification of reaction centers from purple bacteria, in *The Purple Phototrophic Bacteria* (Hunter, C. N., Daldal, F., Thurnauer, M. C., and Beatty, J. T., Eds.), pp 337–353, Springer-Verlag, Dordrecht, The Netherlands.

(50) Tetreault, M., Rongey, S. H., Feher, G., and Okamura, M. Y. (2001) Interaction between cytochrome c_2 and the photosynthetic reaction center from *Rhodobacter sphaeroides*: Effects of charge-modifying mutations on binding and electron transfer. *Biochemistry 40*, 8452−8462.

(51) Gong, X. M., Paddock, M. L., and Okamura, M. Y. (2003) Interactions between cytochrome c_2 and photosynthetic reaction center from *Rhodobacter sphaeroides*: Changes in binding affinity and electron transfer rate due to mutation of interfacial hydrophobic residues are strongly correlated. *Biochemistry 42,* 14492–14500.

(52) Gerencsér, L., and Maróti, P. (2001) Retardation of proton transfer caused by binding of the transition metal ion to the bacterial reaction center is due to pK_a shifts of key protonatable residues. *Biochemistry 40,* 1850–1860.

(53) Williams, J. C., Haffa, A. L. M., McCulley, J. L., Woodbury, N. W., and Allen, J. P. (2001) Electrostatic interactions between charged amino acid residues and the bacteriochlorophyll dimer in reaction centers from *Rhodobacter sphaeroides*. *Biochemistry 40*, 15403–15407.

(54) Tiede, D. M., Vashishta, A. C., and Gunner, M. R. (1993) Electron-transfer and electrostatic properties of the *Rhodobacter sphaeroides* reaction center and soluble *c*-cytochromes. *Biochemistry 32*, 4515−4531.

(55) Tetreault, M., Cusanovich, M., Meyer, T., Axelrod, H., and Okamura, M. Y. (2002) Double mutant studies identify electrostatic interactions that are important for docking cytochrome c_2 onto the bacterial reaction center. *Biochemistry 41*, 5807−5815.

(56) Miyashita, O., Onuchic, J. N., and Okamura, M. Y. (2004) Transition state and encounter complex for fast association of cytochrome c_2 with bacterial reaction center. *Proc. Natl. Acad. U. S. A. 101*, 16174–16179.

(57) Miller, A. F. (2012) Superoxide dismutases: Ancient enzymes and new insights. *FEBS Lett. 586*, 585–595.

(58) Wu, A. J., Penner-Hahn, J. E., and Pecoraro, V. L. (2004) Structural, spectroscopic, and reactivity models for the manganese catalases. *Chem. Rev. 104*, 903–938.

(59) Mukhopadhyay, S., Mandal, S. K., Bhaduri, S., and Armstrong, W. H. (2004) Manganese clusters with relevance to photosystem II. *Chem. Rev. 104*, 3981–4026.

(60) McEvoy, J. P., and Brudvig, G. W. (2006) Water-splitting chemistry of photosystem II. *Chem. Rev. 106*, 4455–4483.

(61) Scarpellini, M., Gätjens, J., Martin, O. J., Kampf, J. W., Sherman, S. E., and Pecoraro, V. L. (2008) Modeling the resting state of oxalate oxidase and oxalate decarboxylase enzymes. *Inorg. Chem. 47*, 3584–3593.

(62) Sjödin, M., Gätjens, J., Tabares, L. C., Thuéry, P., Pecoraro, V. L., and Un, S. (2008) Tuning the redox properties of manganese(II) and its implications to the electrochemistry of manganese and iron superoxide dismutases. *Inorg. Chem. 47*, 2897–2908.

(60) Dhungana, S., Taboy, C. H., Anderson, D. S., Vaughan, K. G., Aisen, P., Mietzner, T. A., and Crumbliss, A. L. (2003) The influence of the synergistic anion on iron chelation by ferric binding protein, a bacterial transferrin. *Proc. Natl. Acad. Sci. U. S. A. 100*, 3659–3664.

(64) Heymann, J. J., Weaver, K. D., Mietzner, T. A., and Crumbliss, A. L. (2007) Sulfate as a synergistic anion facilitating iron binding by the bacterial transferrin FbpA: The origins and effects of anion promiscuity. *J. Am. Chem. Soc. 129*, 9704–9712.

(65) Wraight, C. A. (2006) Chance and design–Proton transfer in water, channels, and bioenergetic proteins. *Biochim. Biophys. Acta 1757*, 886–912.

(66) Tommos, C., and Babcock, G. T. (2000) Proton and hydrogen currents in photosynthetic water oxidation. *Biochim. Biophys. Acta 1458*, 199–219.

(67) Hammes-Schiffer, S. (2015) Proton-coupled electron transfer: Moving together and charging forward. *J. Am. Chem. Soc. 137*, 8860–8871.

(68) Deshmukh, S. S., Williams, J. C., Allen, J. P., and Kálmán, L. (2011) Light-induced conformational changes in photosynthetic reaction centers: Dielectric relaxation in the vicinity of the dimer. *Biochemistry 50*, 340–348.

(69) Deshmukh, S. S., Williams, J. C., Allen, J. P., and Kálmán, L. (2011) Light-induced conformational changes in photosynthetic reaction centers: Redox-regulated proton pathway near the dimer. *Biochemistry 50*, 3321–3331.

(70) Maróti, P., and Wraight, C. A. (1988) Flash-induced H^+ binding by bacterial photosynthetic reaction centers: Influences of the redox states of the acceptor quinones and primary donor. *Biochim. Biophys. Acta 934*, 329–347.

(71) McPherson, P. H., Okamura, M. Y., and Feher, G. (1988) Light-induced proton uptake by photosynthetic reaction centers from *Rhodobacter sphaeroides* R-26. I. Protonation of the one-electron states $D^+Q_A^-$, DQ_A^-, $D^+Q_AQ_B^-$, and $DQ_AQ_B^-$. *Biochim. Biophys. Acta 934*, 348–368.

(72) Allen, J. P., Williams, J. C., Graige, M. S., Paddock, M. L., Labahn, A., Feher, G., and Okamura, M. Y. (1998) Free energy dependence of the direct charge recombination from the primary and secondary quinones in reaction centers from *Rhodobacter sphaeroides*. *Photosynth. Res. 55*, 227–233.

(73) Martin de Rosales, R.T., Faiella, M., Farquhar, E., Que, L.J., Andreozzi, C., Pavone, V., Maglio, O., Nastri, F., and Lombardi, A. (2010) Spectroscopic and metal-binding properties of DF3: an artificial protein able to accommodate different metal ions. *J. Biol. Inorg. Chem. 15*, 717–728.

(74) Kálmán, L., Williams, J. C., and Allen, J. P. (2005) Proton release due to manganese binding and oxidation in modified bacterial reaction centers. *Biochemistry 44*, 13266–13273.

(75) Espiritu, E., Olson, T. L., Williams, J. C., and Allen, J. P. (2017) Binding and energetics of electron transfer between an artificial four-helix Mn-protein and reaction centers from *Rhodobacter sphaeroides. Biochemistry 56,* 6460–6469.

(76) Allen, J. P., Olson, T. L., Oyala, P., Lee, W. J., Tufts, A. A., and Williams, J. C. (2012) Light-driven oxygen production from superoxide by Mn-binding bacterial reaction centers. *Proc. Natl. Acad. Sci. U. S. A. 109,* 2314–2318.

(77) Wydrzynski, T. J., and Satoh, K., Eds. (2005) *Photosystem II: The Light-Driven Water:Plastoquinone Oxidoreductase*, Springer, Dordrecht, The Netherlands.

(78) Allen, J. P., and Williams, J. C. (2011) The evolutionary pathway from anoxygenic to oxygenic photosynthesis examined by comparison of the properties of photosystem II and bacterial reaction centers. *Photosynth. Res. 107,* 59–69.

(79) Umena, Y., Kawakami, K., Shen, J. R., and Kamiya, N. (2011) Crystal Structure of oxygen-evolving photosystem II at a resolution of 1.9 Å structure of PSII. *Nature 473,* 55–60.

(80) Hwang, H. J., McLain, A., Debus, R. J., and Burnap, R. L. (2007) Photoassembly of the manganese cluster in mutants perturbed in the high affinity Mn-binding site of the H_2O-oxidation complex of photosystem II. *Biochemistry 46,* 13648–13657.

(81) Najafpour, M. M., Ehrenberg, T., Wiechen, M., and Kurz, P. (2010) Calcium manganese (III) oxides ($CaMn_2O_4 \bullet xH_2O$) as biomimetic oxygen-evolving catalysts. *Angew. Chem. Int. Ed. 49,* 2233–2237.

(82) Jin, K., Park, J., Lee, J., Yang, K. D., Pradhan, G. K., Sim, U., Jeong, D., Jang, H. L., Park, S., Kim, D., Sung, N. E., Kim, S. H., Han, S., and Nam, K. T. (2014) Hydrated manganese (II) phosphate ($Mn_3(PO_4)_2 \bullet 3H_2O$) as a water oxidation catalyst. *J. Am. Chem. Soc. 136,* 7435–7443.

(83) Najafpour, M. M., Ghobadi, M. Z., Haghighi, B., Tomo, T., Shen, J. R., and Allakhverdiev, S. I. (2015) Comparison of nano-sized Mn oxides with the Mn cluster of photosystem II as a catalysts for water oxidation. *Biochim. Biophys. Acta 1847,* 294–306.

(84) Najafpour, M. M., Ghobadi, M. Z., Larkum, A. W., Shen, J. R., and Allakhverdiev, S. I. (2015) The biological water-oxidizing complex at the nano-bio interface. *Trends Plant Sci. 20,* 559–568.

(85) Zahran, Z. N., Mohamed, E. A., Ohta, T., and Naruta, Y. (2016) Electrocatalytic water oxidation by a highly active and robust αMn_2O_3 thin film sintered on a fluorine-doped tin oxide electrode. *Chem. Cat. Chem. 8,* 532–535.

(86) Chen, X., Zaro, J. L., and Shen, W. C. (2013) Fusion protein linkers: Property, design, and functionality. *Adv. Drug Deliv. Rev. 65*, 1357–1369.

(87) Goldsmith, J. O., and Boxer, S. G. (1996) Rapid isolation of bacterial photosynthetic reaction centers with an engineered poly-histidine tag. *Biochim. Biophys. Acta 1276*, 171–175.

(88) Haffa, A. L. M., Lin, S., Katilius, E., Williams, J. C., Taguchi, A. K. W., Allen, J. P., and Woodbury, N. W. (2002) The dependence of the initial electron-transfer rate on driving force in *Rhodobacter sphaeroides* reaction centers. *J. Phys. Chem B 106*, 7376–7384.

(89) Artamonova, I. V., Gorichev, I. G., and Godunov, E. B. (2013) Kinetics of manganese oxides dissolution in sulphuric acid solutions containing oxalic acid. *Engineering 5*, 714–719.

(90) Ono, T. (2001) Metallo-radical hypothesis for photoassembly of the $(Mn)_4$-cluster of photosynthetic oxygen evolving complex. *Biochim. Biophys. Acta 1503*, 40–51.

(91) Dismukes, C. G., Ananyev, G., and Watt, R. (2005) Photo-assembly of the catalytic manganese cluster, in *Photosystem II* (Wydrzynski, T., Satoh, K., and Freeman, J., Eds.), pp 609–626, Springer, Dordrecht, The Netherlands.

(92) Najafpour, M. M., Renger, G., Hołyńska, M., Moghaddam, A. N., Aro, E. M., Carpentier, R., Nishihara, H., Eaton-Rye, J. J., Shen, J. R., and Allakhverdiev, S. I. (2016) Manganese compounds as water-oxidizing catalysts: From the natural water-oxidizing complex to nanosized manganese oxide structures. *Chem Rev. 116*, 2886–2936.

(93) Sauer, K., and Yachandra, V. K. (2002) A possible evolutionary origin for the Mn_4 cluster of the photosynthetic water oxidation complex from natural MnO_2 precipitates in the early ocean. *Proc. Natl. Acad. Sci. U. S. A. 99*, 8631–8636.

(94) Russell, M. J., and Hall, A. J. (2002) From geochemistry to biochemistry: Chemiosmotic coupling and transition element clusters in the onset of life and photosynthesis. *Geochem. News 113*, 6–12.

(95) Russell, M. J., Allen, J. F., and Milner-White, E. J. (2008) Inorganic complexes enabled the onset of life and oxygenic photosynthesis, in *Photosynthesis. Energy from the Sun: 14th International Congress on Photosynthesis* (Allen, J. F., Gantt, E., Golbeck, J. H., and Osmond, B., Eds.), pp 1187–1192, Springer, Dordrecht, The Netherlands.

(96) Najafpour, M. M. (2011) Amorphous manganese-calcium oxides as a possible evolutionary origin for the $CaMn_4$ cluster in photosystem II. *Orig. Life Evol. Biosph. 41*, 237–247.

(97) Najafpour, M. M., Heidari, S., Balaghi, S. E., Hołyńska, M., Sadr, M. H., Soltani, B., Khatamian, M., Larkum, A. W., and Allakhverdiev, S. I. (2017) Proposed mechanisms for water oxidation by photosystem II and nanosized manganese oxides. *Biochim. Biophys. Acta 1858*, 156–174.

(98) Reig, J. R., Pires, M. M., Snyder, R. A., Wu, Y., Jo, H., Kulp, D. W., Butch, S. E., Calhoun, J. R., Szyperski, T., Solomon, E. I., and DeGrado, W. F. (2012) Alteration of the oxygen-dependent reactivity of *de novo* due ferri proteins. *Nat. Chem. 4*, 900–906.

(99) Takahashi, E. and Wraight, C. A. (1992) Proton and electron transfer in the acceptor quinone complex of *Rhodobacter sphaeroides* reaction centers: characterization of site-directed mutants of the two ionizable residues, Glu^{L212} and Asp^{L213}, in the Q_B binding site. *Biochemistry 31*, 855–866.

APPENDIX A

SUPPLEMENTARY INFORMATION FROM CHAPTER 2

Supplemental Information

The relationship between the dissociation constant, $K_{D,}$ and the total amount of Mn and reaction centers provided in Equation 2.3 has been previously described.[24,52] The derivation is briefly summarized below.

The total concentration of Mn, $[Mn]_t$, is given by the sum of the concentrations of the bound Mn, [Mn:RC], and free in solution, $[Mn]_f$, and the total concentration of reaction centers, $[RC]_t$, is given by the sum of concentration of reaction centers with bound Mn, [Mn:RC], and without Mn, $[RC]_f$:

$$[Mn]_t = [Mn{:}\,RC] + [Mn]_f \tag{A1}$$

$$[RC]_t = [Mn{:}\,RC] + [RC]_f \tag{A2}$$

The value of K_D is related to the concentration of $[Mn]_f$, $[RC]_f$, and [Mn:RC] according to:

$$K_D = \frac{[Mn]_f[RC]_f}{[Mn{:}RC]} \tag{A3}$$

Using Equations A1 and A2, the concentrations of free Mn and unbound reaction centers can be substituted with the concentrations of the total and bound concentrations, yielding:

$$K_D = \frac{([Mn]_t - [Mn{:}RC])([RC]_t - [Mn{:}RC])}{[Mn{:}RC]} \tag{A4}$$

This equation can be re-written in term of [Mn:RC] as:

$$0 = [Mn{:}\,RC]^2 + (-[RC]_t - [Mn]_t - K_D)[Mn{:}\,RC] + [RC]_t[Mn]_t \tag{A5}$$

Using Equation B2 to substitute $[RC]_f$ for [Mn:RC] yields:

$$0 = [RC]_f{}^2 + (-[RC]_t + [Mn]_t + K_D)[RC]_f - [RC]_t K_D \tag{A6}$$

Solving these two quadratic equations (Equations A5 and A6) and dividing by the total concentration of reaction centers gives the relative concentrations of reaction centers with and without bound Mn:

$$\frac{[Mn{:}\,RC]}{[RC]_t} = \frac{([RC]_t + [Mn]_t + K_D) \pm \sqrt{([RC]_t + [Mn]_t + K_D)^2 - 4[RC]_t[Mn]_t}}{2[RC]_t} \tag{A7}$$

$$\frac{[RC]_f}{[RC]_t} = \frac{([RC]_t - [Mn]_t - K_D) \pm \sqrt{(-[RC]_t + [Mn]_t + K_D)^2 + 4[RC]_t K_D}}{2[RC]_t} \tag{A8}$$

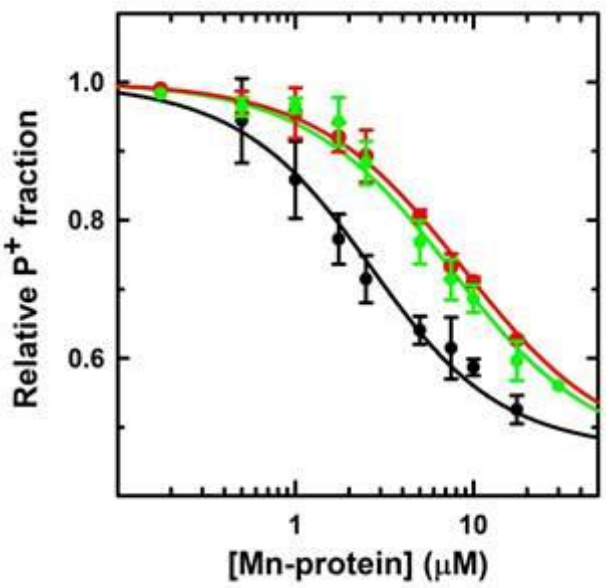

Figure A1. Titrations of HHHH reaction centers with the P1 (black), P1-1 (red) and P1-2 (green) Mn-proteins. The data from three titrations were averaged and fit to Equation 2.3 with the value of *B* constrained to 0.46, yielding K_D values of 1.9, 8.0 and 6.7 μM for the P1, P1-1 and P1-2 Mn-proteins, respectively (Table A1). The value of 0.46 for *B* represents the average of the *B* values obtained for fits of the titrations of the P1, P1-1 and P1-2 Mn-proteins in which *B* is a free parameter (Figure 2.5, Table 2.1).

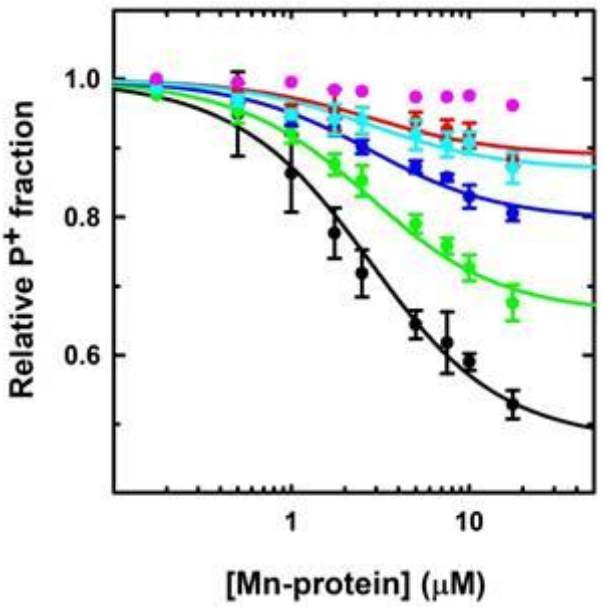

Figure A2. Titrations of reaction centers having different P/P^+ midpoint potentials with the P1 Mn-protein. Shown are HFLF (pink), HHDF (red), HHEF (cyan), HHHF (blue), HHLH (green) and HHHH (black) reaction centers, with $E_m^{P/P+}$ values of 468, 603, 618, 620, 693, and 748 mV, respectively. Fits to the average of three titrations to Equation 2.3 in which the value of K_D was constrained to 2.0 yielded B values (Table A2), similar to the values of the unconstrained fits (Figure 2.7, Table 2.1).

Table A1. Dissociation constants obtained from fits of titrations of HHHH reaction centers with Mn-proteins with *B* constrained.

Mn-protein	Reaction Center	$E_m^{P/P+}$ (mV)[a]	pH	K_D (μM)	B[b]
P1	HHHH	748	9.4	1.9 ± 0.2	0.46
P1-1	HHHH	748	9.4	8.0 ± 0.3	0.46
P1-2	HHHH	748	9.4	6.7 ± 0.7	0.46

[a]The P/P^+ midpoint potential of the HHHH reaction center was measured at pH 8.0 and adjusted to pH 9.4 by –12 mV/pH unit.[14,53]
[b]The *B* value was constrained to be 0.46, the average of the *B* values for the fits in which *B* is not constrained (Table 2.1).

Table A2. Extents of bleaching at high Mn-protein concentration obtained from fits of titrations of reaction centers with the P1 Mn-protein with K_D constrained.

Mn-protein	Reaction Center[a]	$E_m^{P/P+}$ (mV)[b]	pH	K_D (μM)[c]	*B*
P1	HHHH	748	9.4	2.0	0.47 ± 0.01
P1	HHLH	693	9.4	2.0	0.66 ± 0.01
P1	HHEF	620	9.4	2.0	0.87 ± 0.01
P1	HHHF	618	9.4	2.0	0.79 ± 0.01
P1	HHDF	603	9.4	2.0	0.89 ± 0.01

[a]The reaction centers have His, Leu, Glu, Asp, or Phe at residues L131, L168, M160, and M197, designated in order.
[b]The P/P^+ midpoint potentials of the reaction centers were measured at pH 8.0 and have been adjusted to pH 9.4 by –12 mV/pH unit.[14,44,53]
[c]The K_D value was constrained to be 2.0 μM, the average value for the fits in which K_D is not constrained (Table 2.1).

APPENDIX B

SUPPLEMENTARY INOFRMATION FROM CHAPTER 4

Supplemental Information

Figure B1. DNA sequence of NcoI-BamHI fragment used in the construction of the M-D1 fusion proteins.

MD1-3 and MD1-4

```
CCATGGGTTTCAACGCCACGATGGAAGGCATCCACCGCTGGGCCATCTGGATGGCGGTC
C
TCGTGACCCTCACCGGCGGCATCGGCATCCTGCTCTCGGGCACGGTCGTGGACAACTGG
T
ACGTCTGGGGCCAGAACCACGGCATGGCGCCGCTGAACGGCGGGAACGGCGGGAACACC
T
GGGCCGACATCATCAACCGCGCCAACCTGGGCATGGAGGTGATGCACGAGCGCAACGCC
C
ACAACTTCCCGCTGGACCTGGACGGCGGCCACCACCATCATCATCACCACTGAGGATCC
```

MD1-6 and MD1-7

```
CCATGGGTTTCAACGCCACGATGGAAGGCATCCACCGCTGGGCCATCTGGATGGCGGTC
C
TCGTGACCCTCACCGGCGGCATCGGCATCCTGCTCTCGGGCACGGTCGTGGACAACTGG
T
ACGTCTGGGGCCAGAACCACGGCATGGCGCCGCTGAACGGCGGGAACGGCGGGAACACC
T
GGGCCGACATCATCAACCGCGCCAACCTGGGCATGGAGGTGATGCACGAGCGCAACGCC
C
ACAACTTCCCGCTGGACCTGGCCTGAGGATCC
```

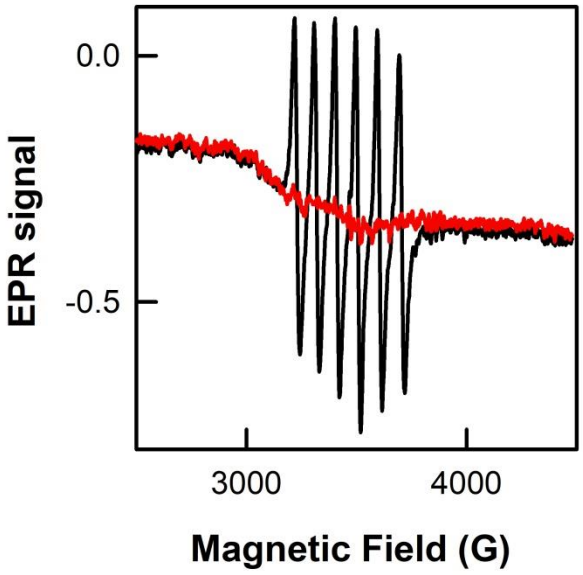

Figure B2. Room temperature EPR data of $MnCl_2$ and $CaMn_2O_4$ stocks in water. EPR data of 100 μM $MnCl_2$ (black trace) and 100 μM suspension of $CaMn_2O_4$ (red trace) in ultra-pure water show a Mn^{2+} EPR signal in $MnCl_2$ and no Mn^{2+} EPR signal in the $CaMn_2O_4$ suspension. The EPR conditions were the following: room temperature, X-band and 1 mW power with an average of 16 scans.

Table B1. C-terminal region of mutant reaction centers

Wild Type	MAPL
MD1-3	MAPLNGGNGGNTWADIINRANLGMEVMHERNAHNFPLDLA
MD1-4	MAPLNGGNGGNTWADIINRANLGMEVMHERNAHNFPLDLA
MD1-6	MAPLNGGNGGNTWADIINRANLGMEVMHERNAHNFPLDLDGGHHHHHHH
MD1-7	MAPLNGGNGGNTWADIINRANLGMEVMHERNAHNFPLDLDGGHHHHHHH
D1	SVIDAKGNVINTWADIINRANLGMEVMHERNAHNFPLDLA

Table B2. Mutations of single amino acid residues of mutant reaction centers

	L131	M160	M197	M164	M168	M173	M192	M288
Wild Type	Leu	Leu	Phe	Arg	Met	Glu	Val	Gly
T1	His	His	His	Arg	Met	Glu	Val	Gly
Mn12	His	His	His	Tyr	Glu	Glu	Val	Asp
Mn28	His	His	His	Tyr	Glu	His	Glu	Asp
Mn31	His	His	His	Tyr	Met	Glu	Glu	Gly
MD1-3	His	His	His	Tyr	Met	Glu	Glu	Gly
MD1-6	His	His	His	Tyr	Met	Glu	Glu	Gly
Mn41	His	His	His	Tyr	Met	Asp	Glu	Gly
MD1-4	His	His	His	Tyr	Met	Asp	Glu	Gly
MD1-7	His	His	His	Tyr	Met	Asp	Glu	Gly

Table B3. Relative P^+ fraction values at a 50 μM concentration of Mn-compounds.

Reaction center	P^+ fraction					
	MnO_2	$CaMn_2O_4$	αMn_2O_3	Mn_3O_4	$Mn_3(PO_4)_2$	$MnCl_2$
WT	1.01 ± 0.03	1.02 ± 0.01	1.02 ± 0.01	1.00 ± 0.02	1.06 ± 0.02	1.07 ± 0.02
T1	1.00 ± 0.05	0.96 ± 0.10	0.85 ± 0.03	0.94 ± 0.08	0.68 ± 0.03	0.57 ± 0.04
Mn12	0.73 ± 0.06	0.10 ± 0.02	0.03 ± 0.01	0.71 ± 0.10	0.01 ± 0.01	0.01 ± 0.01
Mn28	0.58 ± 0.10	0.03 ± 0.02	0.01 ± 0.01	0.41 ± 0.14	0.01 ± 0.01	0.00 ± 0.01
Mn31	0.69 ± 0.05	0.53 ± 0.04	0.21 ± 0.02	0.60 ± 0.03	0.16 ± 0.01	0.15 ± 0.02
Mn41	0.86 ± 0.03	0.58 ± 0.02	0.29 ± 0.02	0.74 ± 0.06	0.21 ± 0.02	0.17 ± 0.00
MD1-3	0.83 ± 0.09	0.59 ± 0.08	0.28 ± 0.05	063 ± 0.08	0.15 ± 0.01	0.14 ± 0.01
MD1-4	0.91 ± 0.02	0.59 ± 0.05	0.39 ± 0.01	0.72 ± 0.07	0.24 ± 0.03	0.20 ± 0.03
MD1-6	0.44 ± 0.09	0.34 ± 0.05	0.14 ± 0.02	0.63 ± 0.05	0.10 ± 0.00	0.07 ± 0.02
MD1-7	0.72 ± 0.08	0.51 ± 0.08	0.26 ± 0.07	0.70 ± 0.04	0.15 ± 0.01	0.11 ± 0.01